© 2017. Published by The Company of Biologists Ltd | Development (2017) 144, 4704-4719 doi:10.1242/dev.154336

RESEARCH ARTICLE

HNF1B controls epithelial organization and cell polarity during ureteric bud branching and collecting duct morphogenesis

Audrey Desgrange[1,2,*], Claire Heliot[1,2], Ilya Skovorodkin[3], Saad U. Akram[4], Janne Heikkilä[4], Veli-Pekka Ronkainen[5], Ilkka Miinalainen[5], Seppo J. Vainio[3] and Silvia Cereghini[1,2,*]

ABSTRACT

Kidney development depends crucially on proper ureteric bud branching giving rise to the entire collecting duct system. The transcription factor HNF1B is required for the early steps of ureteric bud branching, yet the molecular and cellular events regulated by HNF1B are poorly understood. We report that specific removal of *Hnf1b* from the ureteric bud leads to defective cell-cell contacts and apicobasal polarity during the early branching events. High-resolution *ex vivo* imaging combined with a membranous fluorescent reporter strategy show decreased mutant cell rearrangements during mitosis-associated cell dispersal and severe epithelial disorganization. Molecular analysis reveals downregulation of Gdnf-Ret pathway components and suggests that HNF1B acts both upstream and downstream of Ret signaling by directly regulating *Gfra1* and *Etv5*. Subsequently, *Hnf1b* deletion leads to massively mispatterned ureteric tree network, defective collecting duct differentiation and disrupted tissue architecture, which leads to cystogenesis. Consistently, mRNA-seq analysis shows that the most impacted genes encode intrinsic cell-membrane components with transporter activity. Our study uncovers a fundamental and recurring role of HNF1B in epithelial organization during early ureteric bud branching and in further patterning and differentiation of the collecting duct system in mouse.

KEY WORDS: Kidney, Branching morphogenesis, Cell polarity, Transcriptional regulation, *Gdnf-Gfrα1-Ret* pathway, Collecting duct

INTRODUCTION

Branching morphogenesis is the process by which simple epithelium arborizes into an elaborate network. The molecular and cellular events underlying branching morphogenesis have only begun to be characterized. Several genetic studies have shown that the GDNF and FGF pathways are necessary to promote the formation of new branches in different organs (Gjorevski and Nelson, 2010). This process also requires a number of cellular events, such as cell migration, adhesion and proliferation. These are guided by intracellular signaling triggered by stimuli at the cell surface, which lead to active actin cytoskeleton reorganization and extracellular matrix remodeling (Kim and Nelson, 2012).

During definitive mouse kidney development, the ureteric bud (UB) is induced by signals from adjacent metanephric mesenchyme (MM) and emerges from the caudal part of the Wolffian duct (WD) at embryonic day 10.5 (E10.5). This initial outgrowth is regulated by the GDNF/Ret signaling cascade and is mainly due to localized cell proliferation and cell movements into a pseudostratified epithelium (Michael and Davies, 2004; Costantini, 2012). The UB remains pseudostratified during the first branching event (E11.5) and is subsequently reshaped into a simple cuboidal epithelial tube (Chi et al., 2009a). From E11.5 to E15.5, the UB expands into the MM forming new branches and inducing nephrogenesis at each branch tip. After E15.5, UB growth slows and the trunks of the branches elongate, differentiating into principal and intercalated cells (Costantini, 2012). This stereotyped process of branching gives rise to the complex network of collecting ducts (CDs) that will transport the renal filtrate from the nephrons to the ureter and, subsequently, the bladder.

The POU-homeodomain transcription factor HNF1B plays a crucial role in the early differentiation of various cell lineages and organs in vertebrates (Barbacci et al., 1999; Wild et al., 2000; Bohn et al., 2003; Coffinier et al., 2002; Gresh et al., 2004; Haumaitre et al., 2005; Lokmane et al., 2008). In humans, *HNF1B* heterozygous mutations cause the complex syndrome renal cysts and diabetes (RCAD) that is characterized by kidney, genital tract and pancreas abnormalities, as well as early onset of diabetes (Barbacci et al., 2004; Bellanné-Chantelot et al., 2004; Haumaitre et al., 2006; Heidet et al., 2010). Constitutive inactivation in the epiblast by tetraploid aggregation has shown that HNF1B is involved in WD maintenance, the timing of UB outgrowth and its early branching, as well as in the induction of nephrogenesis (Lokmane et al., 2010). However, the premature arrest of UB growth after the first branching event in these tetraploid rescued embryos precluded the examination of later aspects of branching and CD morphogenesis (Lokmane et al., 2008, 2010).

Using conditional inactivation in nephron progenitors, we uncovered an additional and later role of HNF1B in the acquisition of a proximal-intermediate nephron segment fate and subsequent differentiation of all nephron segments (Heliot et al., 2013). This function appears to be conserved in vertebrates (Heliot et al., 2013; Massa et al., 2013; Naylor et al., 2012). It has also been shown that *Hnf1b* conditional inactivation in renal medullar tubules leads to cystic kidneys after birth (Gresh et al., 2004; Hiesberger et al., 2005). Importantly, human fetuses carrying heterozygous mutations in *HNF1B* exhibited bilateral dysplastic kidneys with cysts derived from all nephron segments and the collecting system (Haumaitre et al., 2006), thus indicating an early developmental role in human kidney morphogenesis. However, and despite previous studies, the role of this factor during CD morphogenesis has not yet been addressed.

Here, we examine the function of HNF1B during renal branching using conditional inactivation in the UB and its derivatives. By

[1]Sorbonne Universités, UPMC Université Paris 06, IBPS – UMR7622, F-75005 Paris, France. [2]CNRS, UMR7622, Institut de Biologie Paris-Seine (IBPS) – Developmental Biology Laboratory, F-75005 Paris, France. [3]Faculty of Biochemistry and Molecular Medicine, Biocenter, University of Oulu; Laboratory of Developmental Biology, Biocenter Oulu and InfoTech, Department of Medical Biochemistry and Molecular Medicine, Oulu Center for Cell Matrix Research, 90220 Oulu, Finland. [4]Center for Machine Vision Research and Signal Analysis (CMVS), University of Oulu, FIN-90014, Oulu, Finland. [5]Biocenter Oulu, University of Oulu, FIN-90014, Oulu, Finland.

*Authors for correspondence (audrey.dsg@gmail.com; silvia.cereghini@upmc.fr)

A.D., 0000-0001-9716-755X; S.C., 0000-0002-1562-089X

Received 9 May 2017; Accepted 3 November 2017

Development (2017) 144, 4704-4719 doi:10.1242/dev.154336

using a reporter strategy that allows high-resolution analysis of cell behaviors, we show that deletion of *Hnf1b* affects cell movements during mitosis. We found that HNF1B is required both at the tip domain to maintain cell-cell contacts and within the UB trunks for proper epithelial cell organization and further differentiation of the collecting system.

RESULTS

Hnf1b inactivation in the ureteric bud and derivatives leads to severe urogenital tract abnormalities

To examine the specific function of HNF1B during UB branching, we used the *HoxB7-Cre* line that mediates recombination in the WD and derivatives from E9.5 (Yu et al., 2002). We assessed deletion efficiency by generating two mouse lines: one carrying the $ROSA26^{loxP\text{-}mtomato\text{-}loxP\text{-}mEGFP}$ reporter and $Hnf1^{fl/f}$, which expresses the EGFP or tomato marker at the cell membrane, depending on the expression of Cre-recombinase, and the other with the $Rosa^{EYFP/+}$ reporter. HNF1B-GFP co-immunostaining at E13.5 showed the specificity of the deletion in the UB compartment because as developing nephrons, MM and stroma did not express GFP (Fig. 1A,C). As expected, in controls, $HNF1B^{+}$ nuclei were detected in both UB branches and developing nephrons (Fig. 1A). In mutants, HNF1B was present in early nephron structures, whereas no specific HNF1B staining was observed in GFP^{+} cells (Fig. 1B). Accordingly, we found a 30% decrease in wild-type *Hnf1b* transcripts at E13.5 (Fig. 1E). However, some cells were GFP negative and HNF1B positive, apparently owing to a partial mosaicism of the HoxB7-Cre. This mosaic deletion of Hnf1b then allowed us to compare the fate of HNF1B-postitive and HNF1B-negative cells. Interestingly, at E13.5 we found more $HNF1B^{+}$ cells within the mutant tips than in the trunks (59.7% and 24.2%, respectively; Fig. 1F). By contrast, the same proportion of cells from tips or trunks in heterozygous kidneys lacked EYFP staining (12.6% and 11%, respectively). At later stages, $HNF1B^{+}$ cells were almost undetectable in mutant embryos in the future CDs and developing ureter, whereas the percentage at the UP tips increased up to 90%. Thus, mutant cells appear to be progressively excluded from the UB tips to populate the trunks (Fig. 1F). Interestingly, we have previously observed a similar behavior by *Hnf1b* mutant cells in $Hnf1b^{-/-}$: *WT* diploid chimeras (Lokmane et al., 2010).

The extensive cell rearrangements that occur during UB branching likely contribute to the differential mosaicism observed within the tip and trunk domains, which leads to a strong reduction in *Hnf1b* mutant cells within the UB tips while the future CDs contain mostly mutant cells. This differential mosaicism allowed the examination of HNF1B function at later stages during collecting duct morphogenesis.

Gross morphology analyses were performed at different developmental stages and in newborn pups, in controls ($HoxB7^{Cre/+}$; $Hnf1b^{lacZ/+}$) and mutants ($HoxB7^{Cre/+}$;$Hnf1b^{fl/lacZ}$), from the same litter either carrying or lacking the allele $ROSA26^{loxP\text{-}mtomato\text{-}loxP\text{-}mEGFP}$ (see mouse genotype details in the Materials and Methods). Mutant kidneys exhibited delayed UB branching and irregular WDs, often exhibiting ectopic buds, at E13.5 (96%) (Fig. 1D and Fig. 2A′).

Mutant newborns were obtained at the expected Mendelian ratio; however, the majority of them died between P2 and P15 (Table 1). At P0, the mutants displayed multiple urogenital tract abnormalities, including severe bilateral hypoplasia, medullar cysts and hydroureters, and in some cases kidney/ureter duplications or unilateral agenesis (Table 1; Fig. 2B,B′). Further analysis of either E16.5-17.5 mutant embryos or P0 newborns showed normal insertion of the ureters into the bladder in both females and males, with no evidence of ureter obstruction that could explain hydroureters (data not shown). Additionally, mutants exhibited cysts both in the female (oviducts) and male (epididymus) genital tracts (Fig. 2B′ and data not shown).

Histological examination of mutant kidneys showed strongly reduced branching and nephron number, as well as the development of medullar cysts (Fig. 2C-D′). In mutants, nascent nephrons appeared to develop normally as manifested by WT1 expression in future podocytes of well-formed S-shaped bodies (Fig. 2E,E′). However, further differentiation of nephron segments was perturbed. Notably, the clusters of proximal tubules, stained for AQP1, and the primitive loop of Henle, stained for NKCC2, were underdeveloped and partially disorganized (Fig. 2F-G′). This could be, at least in part, a secondary consequence of a mispatterned collecting duct system.

Thus, inactivation of *Hnf1b* in the UB and collecting system leads to severe urogenital phenotypes that resemble congenital anomalies of the kidney and urinary tract (CAKUT), one of the predominant developmental disorders that represents about 30% of the anomalies found during the prenatal period.

HNF1B is required for the UB branching program and patterning of the ureteric tree network

The ureteric tree develops from stereotypical branching events of the UB. The analysis of these events has been advanced by the application of optical projection tomography (OPT) and the development of software to quantify kidney morphometrics (Short et al., 2014). We examined the branching of the UB epithelia at E13.5 and E16 in 3D by OPT using Troma-1 staining the UB trunks and Ezrin enriched at the tips (Fig. 3A-D″). Following OPT, reconstructed mutant kidneys showed a significant decrease in branching morphogenesis at E13.5 (Fig. 3A-B″). At E16, CDs developed cysts mainly around the pelvic area (Fig. 3C-D″). Skeletal and segmental metrics were assessed using the Tree Surveyor program (Short et al., 2013). We observed that the number of segments and tips were decreased at E13.5 (68% and 66%, respectively) (Fig. 3E). Consistently, mutant kidneys exhibited a decrease in kidney ureteric tree volume of 68% at E13.5 (Fig. 3F) and 60% at E16 (not shown). At E11.5 we observed mis-shaped UB tips (157° in control versus 106° in mutants, data not shown) as observed previously (Lokmane et al., 2010). Then, at E13.5, after remodeling, the angle of the first branching event was reduced by 26° in mutants (Fig. 3G). When assessing all branch segments per generation, a significant dysmorphology was observed in the mutant kidneys, as indicated by the decreased volume and the more curved segments (Fig. 3H,I). All together, this analysis shows that deletion of *Hnf1b* in WD and UB causes significant changes in the spatial morphology of the ureteric tree, highlighting the requirement of HNF1B for the UB branching pattern program. These results also suggest that HNF1B is necessary for ureteric tree epithelial organization. These early defects likely affect the later kidney growth and function observed in our mutants.

HNF1B acts both at the tip domain and in the UB stalks to maintain cell organization

To further understand UB branching defects, we used the $ROSA26^{loxP\text{-}mtomato\text{-}loxP\text{-}mEGFP}$ reporter system to investigate the behavior of mutant cells versus wild type during UB branching by time-lapse imaging of *ex vivo* mouse kidney cultures (Movies 1 and 2) using the novel culture method FiZD (Fixed Z-dimension) (Saarela et al., 2017). First, we confirmed the decreased branching and differential cell recruitment phenotypes that were observed in

Development (2017) 144, 4704-4719 doi:10.1242/dev.154336

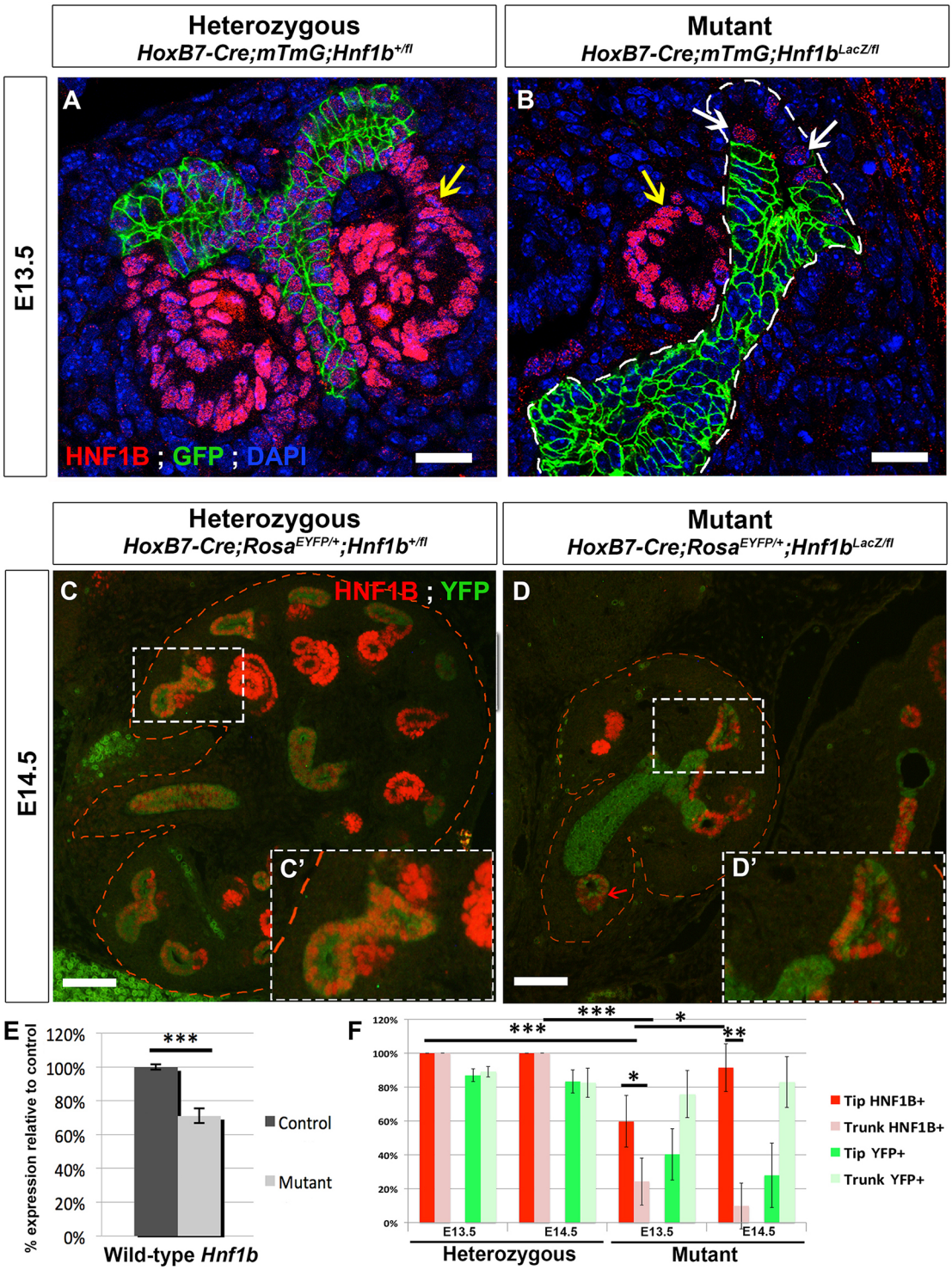

Fig. 1. Conditional deletion of *Hnf1b* in ureteric bud derivatives. (A-D′) Immunostaining of GFP and HNF1B at E13.5 (A,B) and E14.5 (C-D′) shows specific but incomplete loss of HNF1B in mutant UB branches; but also cell sorting of HNF1B^{+}/GFP^{-} cells at the tip domain (compare magnification of UB tip in C′ and D′). Yellow arrows indicate developing nephrons; white arrows indicate HNF1B^{+}/GFP^{-} cells. White dashed line outlines developing UB in B; red dashed line outlines the kidney in C,D. Red arrow in D shows ectopic bud from the WD. Scale bars: 20 µm in A,B; 100 µm in C,D. (E) qRT-PCR of wild-type *Hnf1b* transcripts in control (n=6) and mutant (n=8) kidneys at E13.5 (n being a pool of the two embryo kidneys). (F) GFP/HNF1B immunostained sections were used to quantify mosaicism: HNF1B staining shows 60% reduction in mutant kidneys compared with heterozygous. Mutant tips and trunks have significantly different levels of mosaicism with an enrichment of HNF1B^{+} cells within the tips at E14.5 (n=8 heterozygous sections, n=4 mutant sections). *P<0.05, **P<0.01, ***P<0.001; data are mean±s.e.m.

mutant kidneys *in vivo*; indeed, after 56 h or 5 days of culture, mutant kidneys were significantly less branched than controls (compare Movies 1 and 2; Fig. 4A-D′). In addition, while GFP^{+} and GFP^{-} cells were randomly distributed within the UB trunks and tips in the controls. By contrast, mutant cells (GFP^{+}) were increasingly excluded from the UB tip domain (Fig. 4C-D′). Moreover, the epithelial organization of UB branches was also defective, and the lumen was barely detectable in some regions of UB trunks (Fig. 4C,D′).

Development (2017) 144, 4704-4719 doi:10.1242/dev.154336

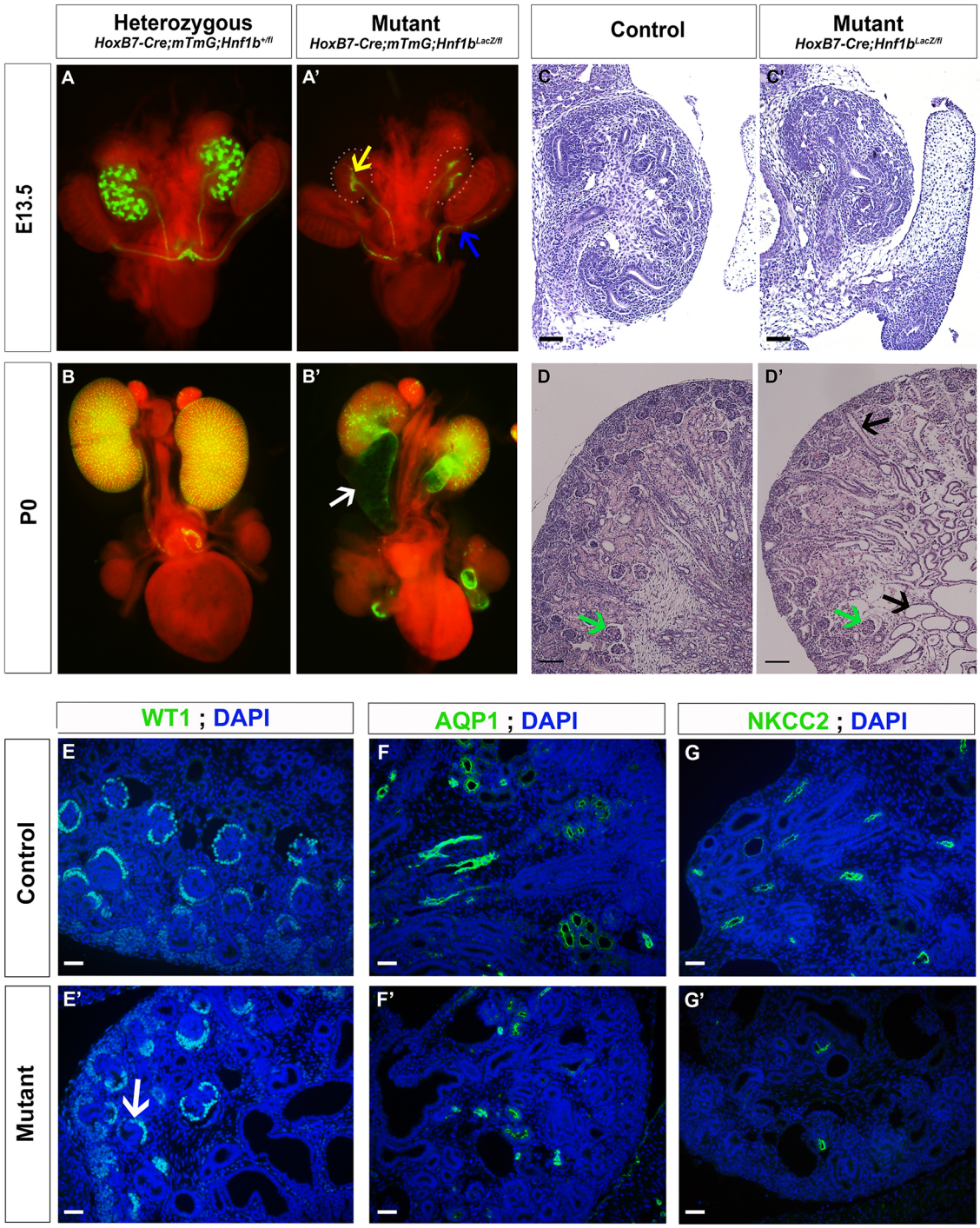

Fig. 2. *Hnf1b* inactivation in Wolffian duct and ureteric bud leads to a wide range of urogenital defects. (A,A′) mTmG expression at E13.5 shows delayed ureteric bud branching (yellow arrow) and Wolffian duct disorganization (blue arrow). Mutant metanephroi are indicated with a dashed line. (B,B′) mTmG expression at P0 shows kidney hypoplasia, hydro-ureter (white arrow) and genital tract duct dilatations. (C-D′) Hematoxylin and Eosin staining at E13.5 and P0 shows delayed branching and tubule dilatation (black arrows) in mutant. Glomeruli appeared well developed (green arrows). (E-G′) Podocytes stained for WT1 (E,E′), proximal tubule stained for AQP1 (F,F′) and Henle's loop stained for NKKC2 (G,G′). Complete differentiation but disorganization of the nephrons in mutants. White arrow in E′ indicates staining in the proximal region of a developing nephron. Scale bars: 40 µm in C,C′,E-G′; 100 µm in D,D′.

These results confirm that *Hnf1b*-deficient cells have a cell-autonomous deficiency in their ability to contribute to the UB tips.

Active cell proliferation occurs at the UB tips, which are major sites for the generation of new branches formed through bifurcation events (Michael and Davies, 2004; Watanabe and Costantini, 2004). After quantifying phosphorylated-histone H3 staining, we did not detect any difference between control and mutant UBs at E12.5 (data not shown). As proliferation is a very dynamic process, we also developed computational parameters to detect mitotic GFP^{+} cells in time-lapse movies. Automated detection (Fig. 5A) and quantification of the proliferation rate showed no significant difference in the first hours of kidney culture (Fig. 5B). As recently reported, UB tip cells exhibit mitosis-associated cell dispersal (MACD) (Packard et al., 2013), a process that has also been observed in other branching

Development (2017) 144, 4704-4719 doi:10.1242/dev.154336

Table 1. Genotypes of newborn pups at P0 and P15, and phenotypes observed at P0

	Control		Heterozygous	Mutant
Genotype	*Hnf1b*$^{+/flx}$ (%)	*Hnf1b*$^{lacZ/flx}$ (%)	*Hoxb7cre; Hnf1b*$^{+/flx}$ (%)	*Hoxb7cre; Hnf1b*$^{lacZ/flx}$ (%)
P0 newborns (*n*=69)	24.69	17.34	30.43	27.54
P15 mice (*n*=60)	30.00	31.67	35.00	3.33
Phenotypes at P0	Control (%)		Heterozygous (%)	Mutant (%)
Kidney hypoplasia	0		0	100
Unilateral agenesis	0		0	10.53
Ureter/kidney duplication	0		0	15.79
Mono- or bilateral hydroureter	0		0	78.95
Number of animals	*n*=29		*n*=21	*n*=19

organs, such as the pancreas (Shih et al., 2016). During MACD, premitotic cells delaminate from the epithelium into the lumen where they divide, after which one daughter cell reinserts into the same site, while the other daughter cell reinserts at position one to three cells away (Fig. 5C) (Packard et al., 2013). Occasionally, we observed tips composed of mainly mutant cells. In this context, we found that cells can divide but did not delaminate from the epithelium, and daughter cells did not dissociate from each other (Fig. 5D). This was confirmed by automatic detection and segmentation of mitotic and daughter cells. We found a reduced distance between the position of the former parent and the two daughter cells in mutants compared with controls 25 min after division (6.6 µm and 9.3 µm, respectively), as well as a reduced distance between mutant daughter cells after mitosis compared with control cells (17 µm in controls versus 9.6 µm in mutants) (Fig. 5G,H). Moreover, in a mutant context, the majority of mutant daughter cells remained in contact 25 min after mitosis (17% of shared border in mutants compared with 1% in controls) (Fig. 5H).

Interestingly, when the neighboring cells were mainly wild type, mutant daughter cells were able to separate from each other (Fig. 5E). Quantifications in this context showed that the distances between daughter and parent cells as well as between the two daughter cells were not statistically different from that of control cells. These distances were significantly higher at 15 and 20 min after mitosis when compared with mutant cell behavior in a mutant environment (Fig. 5F,G). Our observations also suggest that proper MACD depends on cell-cell interactions with the neighboring cells. Altogether, these results indicate an early requirement for HNF1B at the tip domain for cell rearrangements and within the trunk to maintain the organization of the epithelium.

HNF1B controls ureteric bud epithelium organization and polarity

Improper epithelial organization and lack of a lumen in mutant UB trunks, led us to analyze apico-basal polarity both *in vivo* and *ex vivo*. PCK and laminin bind to the apical and basal side of the UB, respectively (Fig. 6A-A″). In some regions of the mutant UB, PCK staining was extended along the basolateral sides and there was a strong decrease in basal laminin staining (Fig. 6B-B″). Staining of adjacent sections showed that these regions were GFP^{+} (Fig. 6C). Moreover, staining with the apical polarity protein aPKC revealed that the organization of the tip domain epithelium was impaired in mutant kidneys (Fig. 6D,D′). In addition, qRT-PCR analyses showed that markers of polarized epithelium, *Cdh16* (Thomson and Aronson, 1999), *Pkhd1* (Wang et al., 2004) and *Cys1* (Tao et al., 2009), were strongly downregulated in our mutants at E13.5, before cyst initiation (Fig. 6E). Interestingly, these genes are direct targets of HNF1B (Bai et al., 1995; Gresh et al., 2004; De Vas et al., 2015; C.H. and S.C., unpublished ChIP-seq data on E14.5 kidneys, Table S1; full details of the ChIP-seq data will be published elsewhere).

Transmission electron microscopy (TEM) analysis was performed at E15. We selected mis-shapen ureteric bud tips, which are indicative of being composed primarily of mutant cells, and found that epithelial organization was impaired in these UBs. Indeed, the basement membrane was more diffuse or even undetectable in mutants (Fig. 6F, G, insets 1 and 4). Moreover, lateral cell-cell junctions were impaired as the space between cells was greatly increased (Fig. 6F,G, inset 3 and 6). However, apical tight junctions appeared to form correctly (Fig. 6F,G, insets 2 and 5). Together, these data suggest that HNF1B is necessary to establish UB apico-basal polarity.

Hnf1b deletion leads to defective expression of key regulators of ureteric bud branching

We have previously shown that HNF1B, although not involved in its initial induction in the intermediate mesoderm, directly controls the transcription of *Pax2* in the nephric duct and UB, but not in the adjacent MM (Lokmane et al., 2010). Remarkably, in our mutants, we clearly observed that the E13.5 UB trunks, which were deficient for *Hnf1b*, lacked the expression of *Pax2*, whereas its expression was maintained in the tips that were HNF1B^{+} (Fig. 7A, B), thus confirming that HNF1B positively regulates *Pax2*.

qRT-PCR and *in situ* hybridization analyses at E13.5 showed that *Ret* expression was decreased in UB branches (Fig. 7C,D,G). qRT-PCR also indicated that levels of *Wnt11* were partially reduced in mutant kidneys (Fig. 7G). Besides, in mutants UB tips enriched in GFP-negative cells, co-immunostaining of WNT11 and GFP showed WNT11 at the tip domain, similar to controls (Fig. 7E,F). However, few cells expressing GFP (thus, lacking HNF1B) lacked WNT11 staining (Fig. 7F′). The analysis of HNF1B staining in adjacent sections confirmed expression of HNF1B in those regions WNT11^{+}/GFP^{-} (data not show). Altogether, these results indicate a strict correlation between the presence of HNF1B and WNT11, further suggesting that HNF1B is involved in the maintenance of the GDNF/Ret/Wnt11 regulatory feedback loop (Majumdar et al., 2003).

qRT-PCR analysis indicated that other components of the pathway were similarly downregulated, notably *Gfrα1*. There was, however, a bias in these results, given the observed recruitment of wild-type cells into the mutant tips and also the enrichment of *Ret* and other downstream effectors to the UB tips. We therefore performed similar analysis in *Hnf1b-Sox2-Cre* mutant line (Hayashi et al., 2002), in which *Hnf1b* is inactivated in the epiblast and consequently less mosaic, and found a stronger downregulation of Ret and other components of the pathway, notably *Gfra1* and *Etv5* (Fig. 7G). Our HNF1B-ChIP-seq analysis on E14.5 kidneys (C.H.

Development (2017) 144, 4704-4719 doi:10.1242/dev.154336

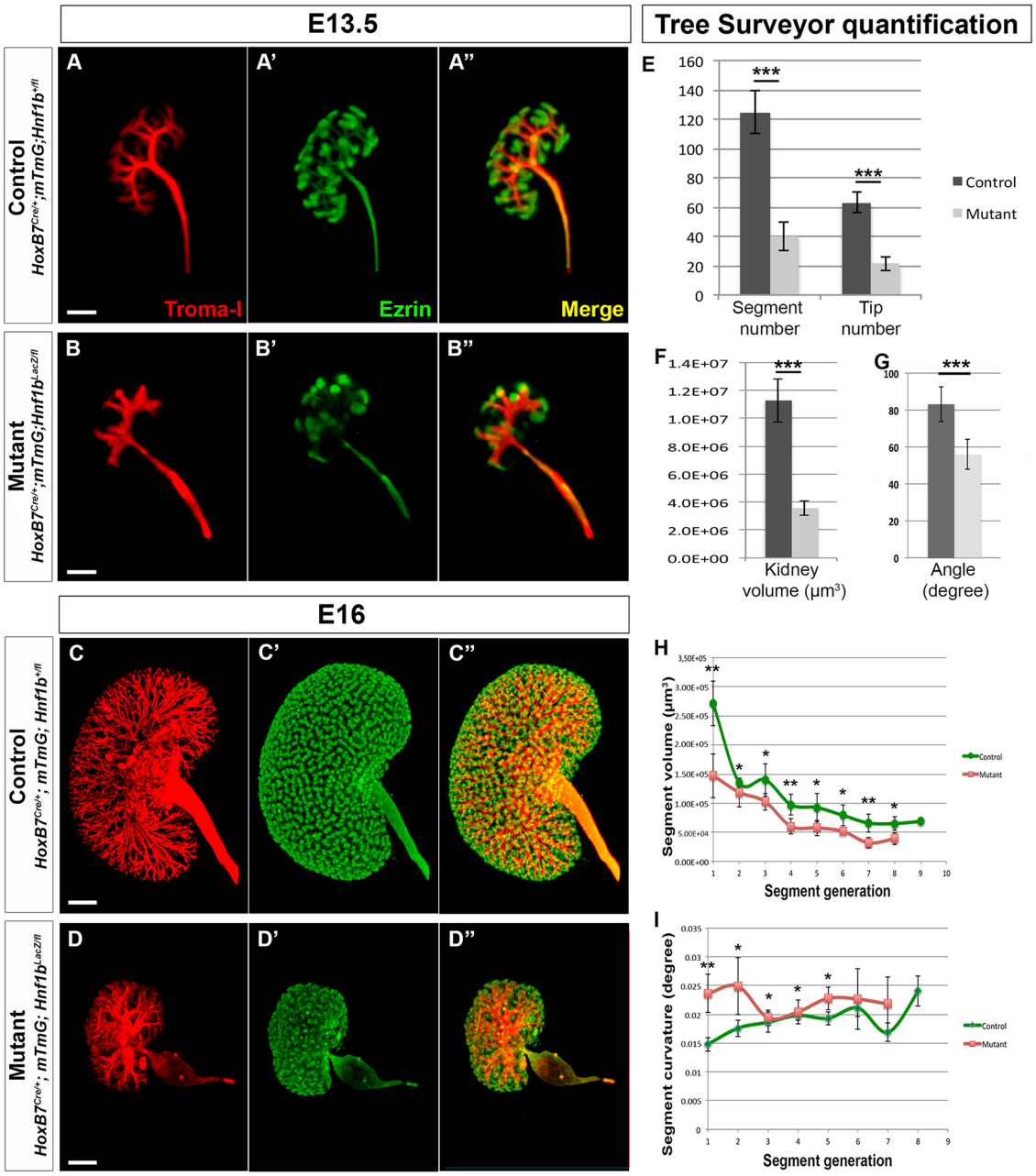

Fig. 3. HNF1B is required to pattern the ureteric tree. (A-D″) Snapshots of optical projection tomography (OPT) scanned kidneys at E13.5 (A-B″) and E16 (C-D″). Troma-1 antibody binds to keratin 8 and shows the apical membrane of ureteric bud branches; ezrin antibody binds strongly at the kidney periphery, showing the ureteric bud tips. Scale bars: 150 µm in A-B″; 300 µm in C-D″. (E-I) Quantitative morphometric analyses of E13.5 mutant and wild-type kidneys using Tree Surveyor. (E,F) Kidney segment, tip number and ureteric tree volume are severely reduced in mutants. A mean value of 124.75 segments was found in controls and 40.25 segments in mutants. A mean of 63.25 tips was found in controls and 21.5 tips in mutants. Control kidney volume was around 1.13×10^7 µm^3, whereas it was only 3.58×10^6 in mutants. (G) The angle of the first branching event at E13.5 is significantly smaller in mutant kidneys (83.5° in control, 56.23° in mutant). (H,I) Segment volume by generation is reduced and global curvature of each segment is increased in mutant kidneys (first generation being the closest branches to the ureter). n=10 controls and 6 mutants. *P<0.05, **P<0.01, ***P<0.001; data are mean±s.e.m.

and S.C., unpublished) indicated that, in addition to the already known targets *Pax2* and *Wnt9b* (Lokmane et al., 2010), HNF1B was bound to the intronic sequences of *Gfra1* and *Etv5* (Gfra1: Chr19: 58470549-58472071: Etv5: chr16: 22428681-22429881) (data not shown). Interestingly, the *Gfra1* and *Etv5* intron sequences are conserved in mammals and contained, respectively, three and one HNF1 consensus binding sites with high motif specificity scores. We confirmed HNF1B binding to these sequences by performing ChIP-qPCR on chromatin isolated from E14.5 mouse kidneys and found that, relative to the IgG control, HNF1B was strongly enriched at both *Gfra1* and *Etv5* peak sequences (Fig. 7H).

We confirmed HNF1B binding to these sequences by performing ChIP-qPCR on chromatin isolated from E14.5 mouse kidneys and found that relative to the IgG control, HNF1B was strongly enriched at both *Gfra1* and *Etv5* peak sequences (by 178.83- and 49.95-fold, respectively) (Fig. 7H).

Altogether, these results show that HNF1B is required for *Pax2* expression in the UB epithelium, and for the maintenance

Development (2017) 144, 4704-4719 doi:10.1242/dev.154336

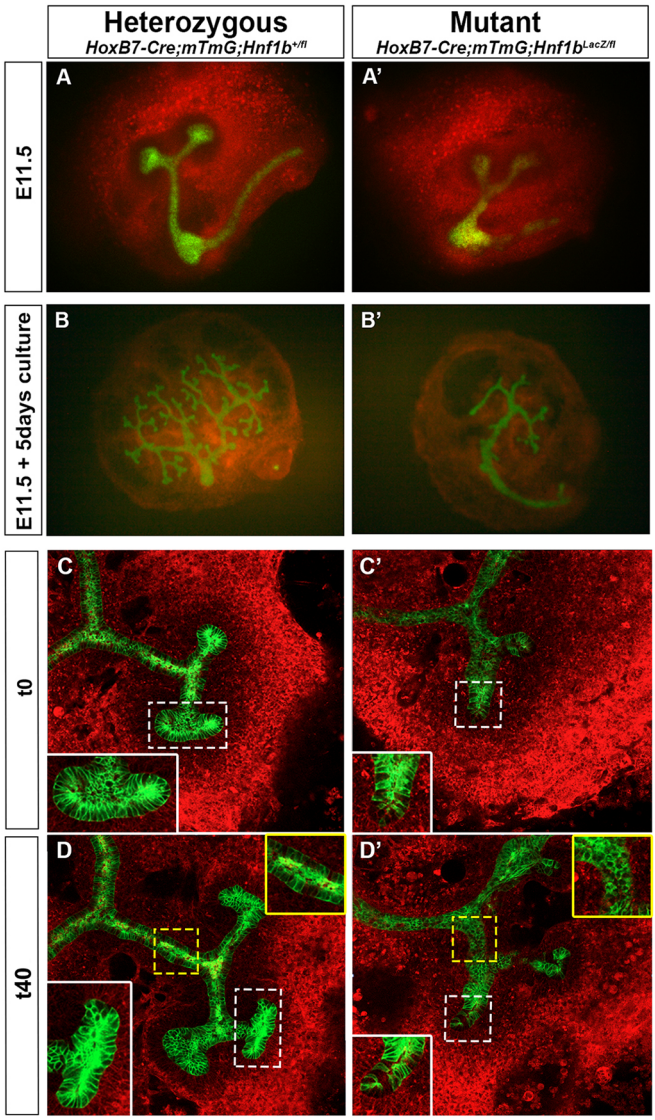

Fig. 4. *Hnf1b* deletion leads to epithelial disorganization and cell rearrangement defects during proliferation. (A-B′) *Ex vivo* culture of heterozygous and mutant kidneys. Kidney culture at day 1 (E11.5) (A,A′) and day 6 (E11.5+5 days) (B,B′). (C-D′) Snapshots of time-lapse imaging of *ex vivo* kidney cultures by FiZD, E11.5+16 h (t0) or +56 h (t40). In this set-up, kidney is flattened and its growth is constrained in the *z*-direction; thus, we can perform high-resolution imaging on fluorescent cells. Red cells (mT) are GFP^- cells, green cells (mG) are GFP^+ cells. White insets show higher magnification of UB tips. Patches of wild-type cells at branching sites are visible in C′ and D′. Yellow insets in D and D′ show higher magnification of epithelial tubular organization. Defective lumen formation is visible in D′.

of key Ret/GDNF pathway components. Our results further suggest that HNF1B transcriptionally regulates *Gfrα1* and *Etv5 in vivo*. Together these molecular misregulations explain, at least at the earlier UB branching steps, the behavior of *Hnf1b*-mutant cells during branching and their inability to contribute to the UB tips.

HNF1B is required to maintain epithelial organization and function of collecting ducts

As shown by histological and OPT analyses, *Hnf1b* mutant kidneys exhibited a severely mispatterned ureteric tree network and developed medullar cysts by E16 (Fig. 2D′ and Fig. 3D-D″). Interestingly dilatations also occurred in the trunk regions of the UB after 3 days of culture (Fig. 4D′ and Movie 2). Immunostaining for E-cadherin (all kidney tubules) and pan-cytokeratin (CDs) at E17.5 showed that the dilated tubules were CDs (Fig. 8A-D′).

Cystogenesis in embryonic kidneys has been reported to be associated with several cellular defects, including increased proliferation, apoptosis, changes in cell-cell and cell-matrix interactions as well as cell polarity (Wilson, 2011). Investigating apicobasal polarity, we found that pan-cytokeratin staining exhibited expanded expression along the basal and lateral regions of mutant CDs, instead of the normal apical localization (Fig. 8D′). Staining with α-acetylated tubulin, a component of cilia, indicated that the percentage of cells with cilia in mutant CDs was significantly reduced compared with controls (−25%) (Fig. 8E-G). In mutant CDs, the apical marker Muc1 was interrupted in several regions of dilated ducts (Fig. 8E,F) and aPKC staining appeared also disorganized and abnormally localized (Fig. 8H,I). Interestingly, similar results were observed *ex vivo*. Troma 1 and laminin, which bind, respectively, to the apical and basal side of the UB trunk, showed a strong decrease in mutant tubules. These regions were specifically GFP^+ and thus, $HNF1B^-$ (Fig. S2). This suggests that the early defects of cell polarity observed in *Hnf1b* mutants affect cilia maintenance. Moreover, neither the water channel AQP2 nor the lectin DBA could be detected in mutants, and the transcript levels of specific markers of principal (*Atp6v1*) and intercalated cells (*Foxi1* and pendrin) were significantly decreased (Fig. 8J-M, see also mRNA-seq data, Table S1), further indicating a global differentiation defect of the CD system. Further analysis of proliferation using the mitosis marker phosphorylated histone H3, showed an increase in the numbers of proliferating cells in the epithelium of mutant CDs when compared with control embryos. At this stage, no change was observed in the number of apoptotic cells assessed by TUNEL (Fig. 8O). These results together suggest that HNF1B acts as a key regulator of UB morphogenesis by exerting direct control over several genes involved in epithelial polarity and ensuring maintenance of tubule size during embryogenesis.

To further elucidate the cellular and molecular components regulated by HNF1B during CD morphogenesis, RNA sequencing was performed on E15.5 control and mutant kidneys, a stage at which the UB trunks were essentially devoid of HNF1B-positive cells and the CDs began to exhibit dilatations. We found that 2511 genes were differentially expressed, of which 328 were upregulated and 499 were downregulated, with a *P*-value (FDR or adjusted *P*-value) of 0.05 and an absolute fold-change cutoff value 1 in a $\log_2$ scale. In contrast to our E13.5 qRT-PCR results, the expression of *Ret* and downstream effectors (*Etv4/5*), as well as *Gfra1*, were essentially not affected at this later stage. This is likely due to the fact that UB tip cells represent a minor number relative to that of the whole kidneys combined with the enrichment of wild-type cells to the tips.

Given the indirect effects upon *Hnf1b* deletion in the collecting system on nephron numbers and their further segment differentiation (Fig. 2), we retrieved from the total list of 499 genes downregulated in whole kidneys, those genes expressed in the UB, cortical and medullar collecting ducts using GUDMAP (www.gudmap.org) (256 genes, Table S1A), and then clustered them using ToppGene informatics (Chen et al., 2009) (Table S2). Remarkably, our RNA-seq data identified several genes differentially expressed with greater fold-changes either in the CDs, including *Tmem27*, *Foxi1*, *Slc26a4* (pendrin), *Slc7a8*, *Slc7a12*, *Slc44a4*, *Scnn1a*, *Kcnj16* and *Aqp2*, or in the medullar CDs and renal pelvis, such as *Foxa1*, *Fxyd3*, *Upk3a*, *Upk2* and *Paqr5*. Unexpectedly, the previously identified targets of HNF1B, such as *Cdh16*, *Pkhd1* and *Crb3* (Verdeguer et al., 2010), *Cys1* and *Glis3* (De Vas et al., 2015), and *Wnt9b* (Lokmane et al., 2010), although downregulated,

Development (2017) 144, 4704-4719 doi:10.1242/dev.154336

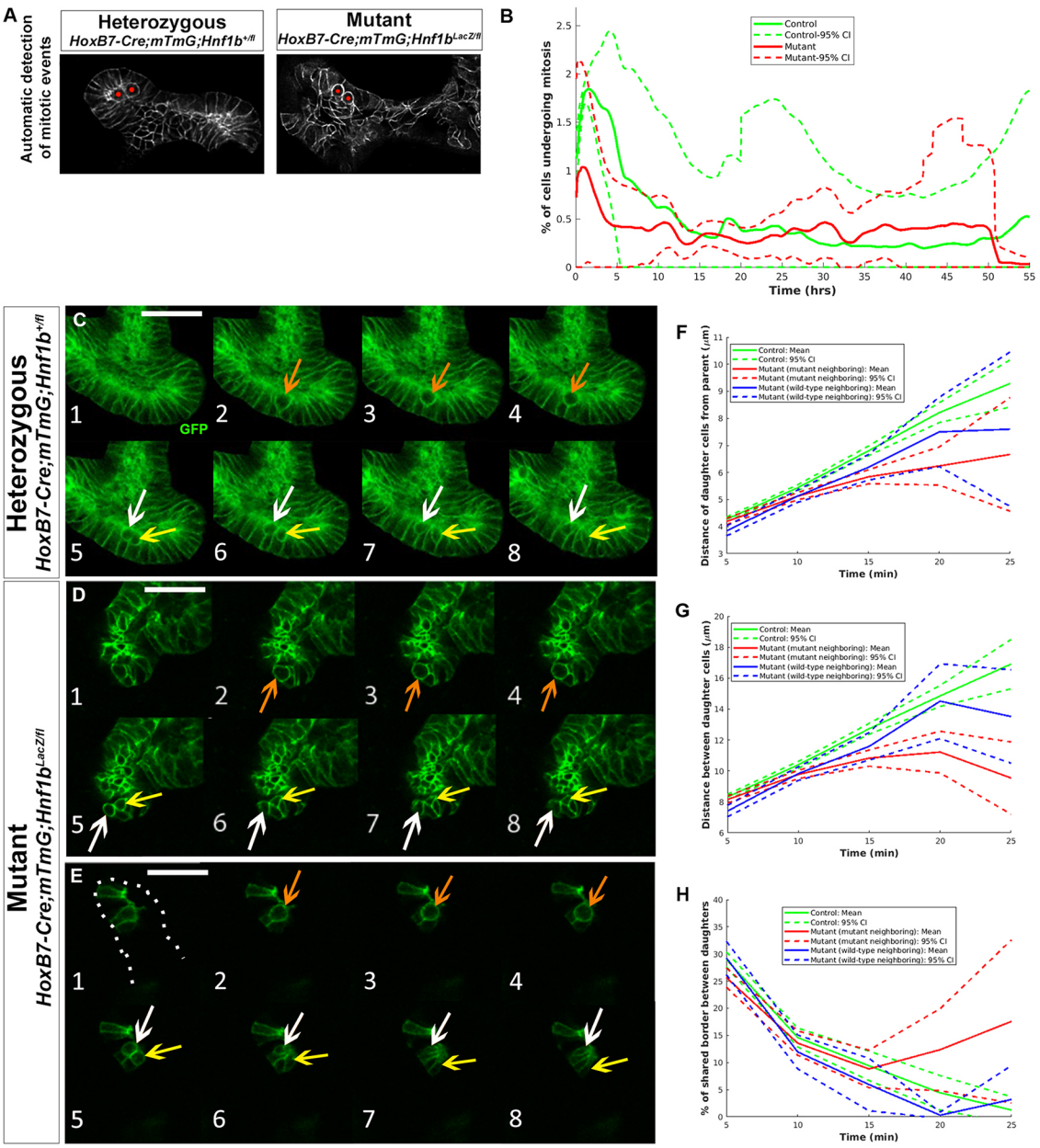

Fig. 5. *Hnf1b* deletion in UB cells does not affect proliferation rate but does affect cell rearrangement after mitosis. Automatic detection of mitotic cells in heterozygous and mutant kidneys (see Materials and Methods). (B) Quantification of mitosis rate over the first 55 h of kidney culture shows no significant difference between control and mutant cells (n=3 controls and 4 mutants). (C-E) Snapshot of time-lapse acquisition of GFP$^+$ cells (GFP); one image was taken every 5 min. Representative images of mitosis in control (C) and mutant UBs (D,E) either in a highly mutant environment (D) or in a wild-type environment (E). White dots in E outline the ureteric bud tip. Orange arrows indicate mother cells; white and yellow arrows indicate daughter cells. Scale bars: 50 µm. (F,G) Tracking of mitotic cells after division: distance between daughter cells and mitosis site (F) or between daughter cells (G). (H) Assessment of the dispersal of the daughter cells was computed as the percentage of shared border over time. 276 cells in two control kidneys and 255 cells (174 in a mutant environment and 81 in a wild-type environment) in four mutant kidneys were tracked.

were all under the cutoff value and therefore not included in the GO analysis (Table S1B).

GO terms included transporter activity, trans-membrane transport, metabolism and lipid metabolic process (Table S2). As expected, several of the downregulated genes had HNF1B consensus binding sites and most of them were found bound by HNF1B by E14.5 kidney-ChIP-seq (C.H. and S.C., unpublished). Notably, the downregulated collecting duct genes were mainly associated with abnormal renal/urinary system physiology, kidney collecting duct epithelium and ureter morphology, as well as hydronephrosis. Of interest among the novel putative HNF1B targets identified (Table S1C) are: the transcription factor Foxa1, which is expressed in the renal and pelvic urothelium and prospective medullar CDs (Yu et al., 2012); the gene encoding the nuclear steroid hormone receptor ESRRG, which is involved in early UB branching and renal papilla development (Berry et al., 2011); *Lgals3*, which is implicated in ureteric bud branching and cyst growth (Bullock et al., 2001; Chiu et al., 2006) as well as the potassium channels *Kcnj1* and *Kcnj16*, *Pdzk1* and several SLC transmembrane transporters, including choline, bicarbonate anion exchanger and metal ion transporters (Table S1C) (Yan et al., 2008; Paulais et al., 2011).

Development (2017) 144, 4704-4719 doi:10.1242/dev.154336

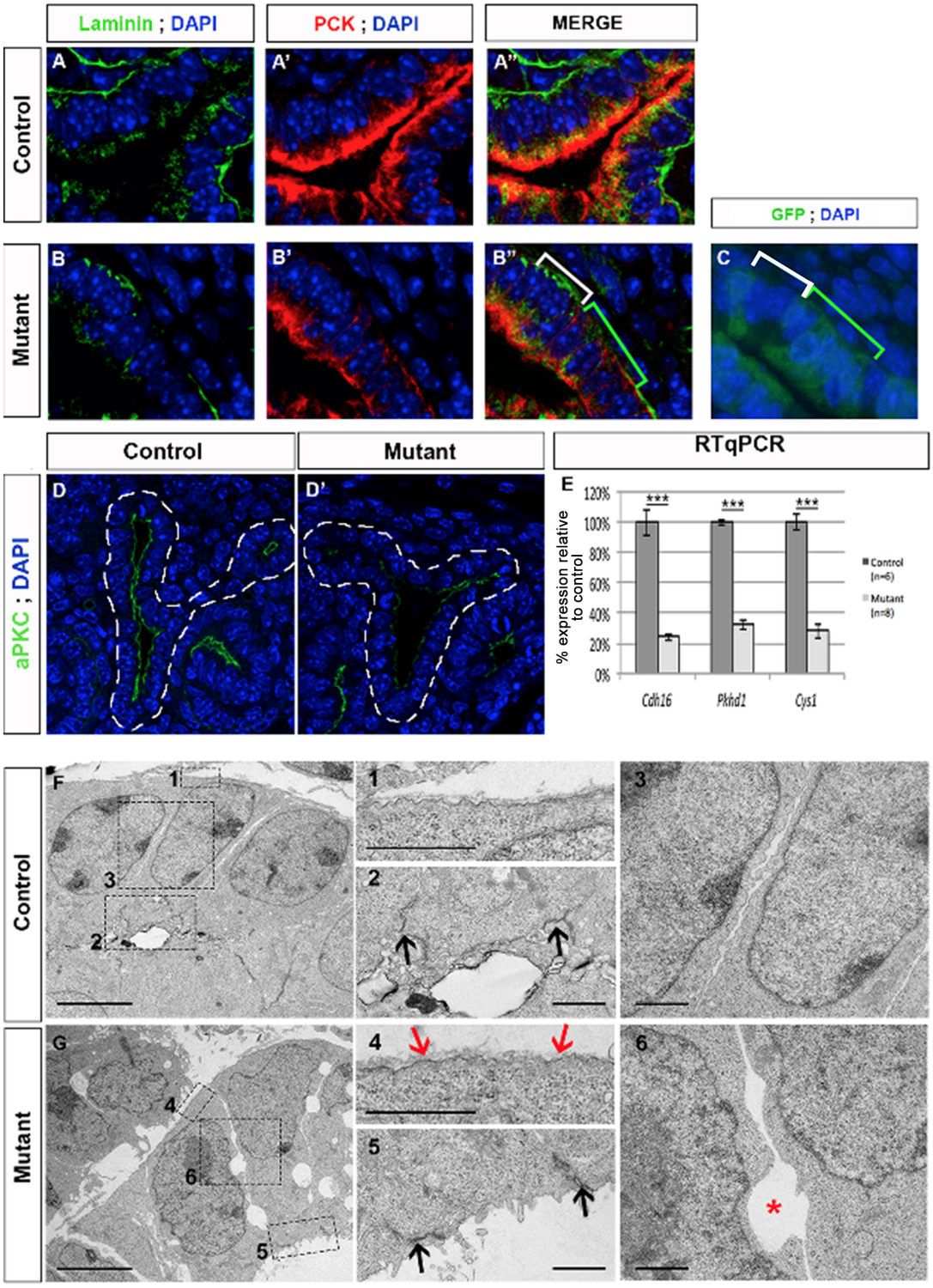

Fig. 6. *Hnf1b* invalidation leads to loss of apicobasal polarity and cell-cell adhesion. (A-C) Confocal images of co-immunohistochemistry for pan-cytokeratin and laminin (A-B″) or HNF1B and GFP (C) on E13.5 kidneys. GFP$^+$ cells in B′ show disruption in basal membrane staining of laminin and expansion of the apical marker PCK to the basolateral sides of the cells. In B″ and C, white brackets indicate GFP$^-$ region, whereas green brackets indicate GFP+ region (mutant cells). (D,D′) Staining of the apical marker aPKC is disorganized in mutant ureteric bud tip. (E) Relative expression of epithelium polarity markers at E13.5 indicates a strong downregulation of these genes in mutant kidneys. *n*=5 controls and *n*=5 mutants (*n* being a pool of the two embryo kidneys). ***P<0.001; data are mean± s.e.m. (F,G) Transmission electron microscopy on E15.5 kidneys shows disorganization of the basal membrane (compare boxes 1 and 4, red arrows) and loss of lateral cell-cell junctions (compare boxes 3 and 6, red star). Tight junctions appeared well organized in both control and mutant kidneys (boxes 2 and 5, arrows).

Consistent with the histological and TEM results at E13.5, cellular component analyses indicated that the most significantly downregulated genes were membrane components, such as the cell-junction markers *Gjb1*, *Cldn19* and *Itgb6*, which are additionally putative HNF1B targets (Table S1C). Interestingly, qRT-PCR at E13.5 showed that these genes were also

Development (2017) 144, 4704-4719 doi:10.1242/dev.154336

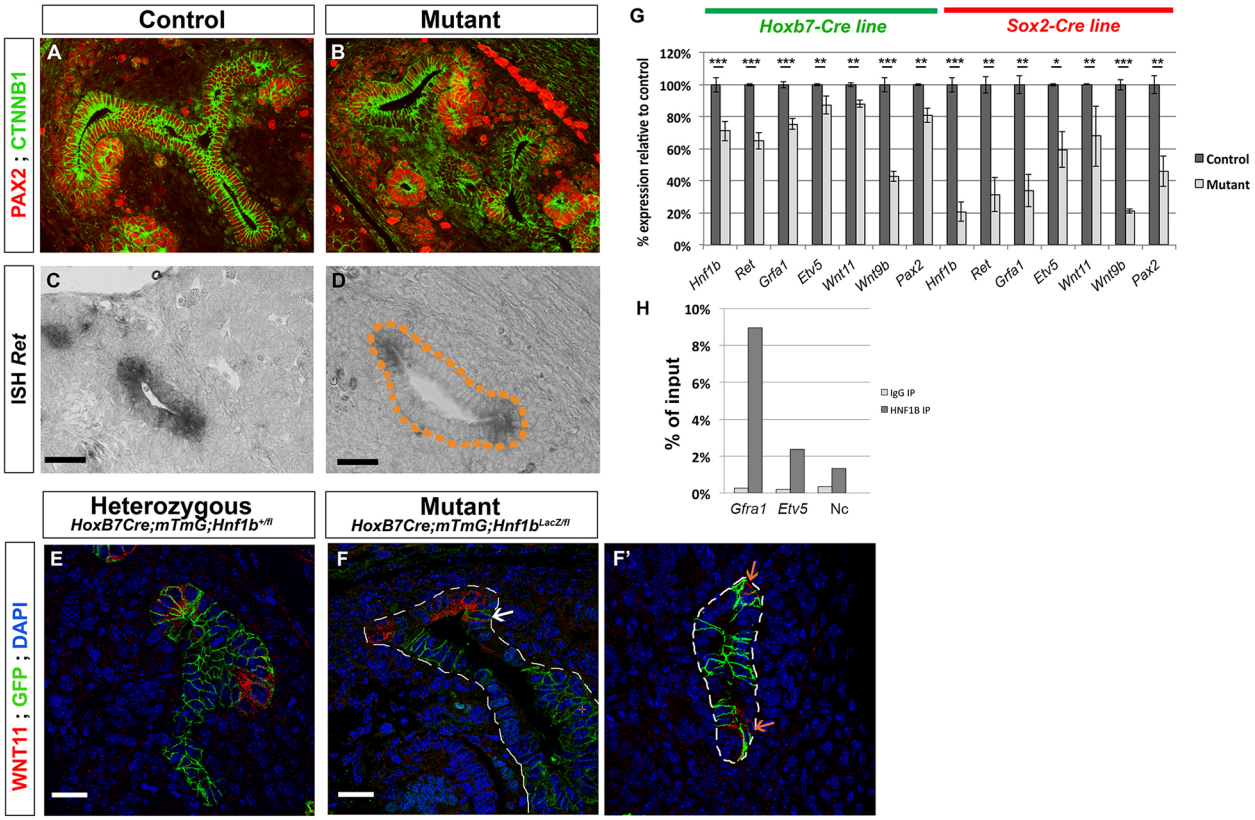

Fig. 7. HNF1B is necessary to maintain Ret and Pax2 expression at the tip domain. (A,B) Immunostaining of PAX2 CTNNB1 at E13.5 shows loss of PAX2 in some regions of ureteric bud. PAX2$^+$ cells are mainly at the tip domain where HNF1B$^+$ cells are also found. (C,D) *In situ* hybridization shows reduced Ret expression in UBs at E13.5. Orange dashed line outlines the UB tip. Scale bars: 40 µm. (E-F′) Immunostaining of WNT11 and GFP at E13.5 shows persistence at the tip domain in mutant kidney, with specific loss of staining in GFP$^+$ cells (white arrow). Orange arrows in F′ show GFP$^-$ cells with WNT11 staining. Scale bars: 20 µm. (G) qRT-PCR of the indicated genes at E13.5 in HoxB7-Cre and Sox2-Cre mutants. *n*=5 controls and 5 mutants for HoxB7-Cre line, *n*=6 controls and 4 mutants for Sox2-Cre line (*n* being a pool of the two embryo kidneys). **P*<0.05, ***P*<0.01, ****P*<0.001; data are mean±s.e.m. (H) qPCR on two independent ChIPs shows HNF1B binding on mouse *Gfra1* and *Etv5* intronic sequences. qPCR on the control IgG and HNF1B ChIP are expressed as percentage of the input. (Nc, negative control, as described by Heliot and Cereghini, 2012).

downregulated at this earlier stage (data not shown). Conversely, the most significantly upregulated genes were cytoskeleton components such as *Mybph* or *Krt5* (Table S1D).

DISCUSSION

Conditional inactivation of *Hnf1b* in the WD and UB derivatives, using the HoxB7cre line, uncovered a crucial role of this transcription factor in cellular organization and epithelial polarity during UB branching and CD morphogenesis. The early mosaic activity exhibited by the *Hoxb7cre* combined with the progressive exclusion of mutant cells from the UB tips allowed both high-resolution imaging of cell behaviors during the early steps of UB branching and the analysis of later functions of HNF1B during collecting duct maturation. We found that mutant embryos displayed severe urogenital phenotypes associated with UB branching defects and abnormal epithelium organization. Together, these data indicate an initial crucial requirement for HNF1B in the acquisition of a UB tip domain and branching, followed by a role in tubular epithelial organization and cortico-medullar organization of the ureteric tree.

Early role in the UB tips: cell rearrangements and apico-basal polarity

In addition to proliferation, active cell movements (requiring constant turnover of cellular adhesions and cytoskeleton) have been implicated in UB morphogenesis (Chi et al., 2009a; Kuure et al., 2010). It has been shown that GDNF/Ret signaling promotes cell movements in the nephric duct that lead to the primary UB (Chi et al., 2009b). Moreover, in chimeric embryos, *Ret* mutant cells are excluded from the nascent tips despite the ureter being populated with them. These cell-sorting behaviors depend in turn on RET-signaling levels, as cells with higher signaling activity migrate more efficiently towards the budding sites (Riccio et al., 2016).

Using a dual fluorescent reporter system, we have been able to describe temporal and dynamic behaviors of mutant and wild-type cells during the branching process. As previously reported using diploid chimeras (Lokmane et al., 2010), we observe that cells lacking *Hnf1b* are progressively excluded from the UB tips, behaving as *Ret*, *Etv4* or *Fgfr2-null* UB cells (Leclerc and Costantini, 2016). Interestingly, the deficiency in the contribution of *Hnf1b* mutant cells to the UB tips appears as severe as that reported for *Ret*$^{-/-}$ cells and higher than that of *Fgfr2*$^{-/-}$ (Chi et al., 2009b). Altogether, these observations suggest that HNF1B acts cell-autonomously to establish a specialized tip domain.

We found decreased expression of some GDNF/Ret signaling components in E13.5 mutants, which together may contribute to the abnormal UB cell rearrangements and defective branching phenotype observed. Notably, we showed that HNF1B is a transcriptional regulator of *Gfra1* and *Etv5*. It is interesting to note that HNF1B acts at several levels of the GDNF/Ret cascade as

Development (2017) 144, 4704-4719 doi:10.1242/dev.154336

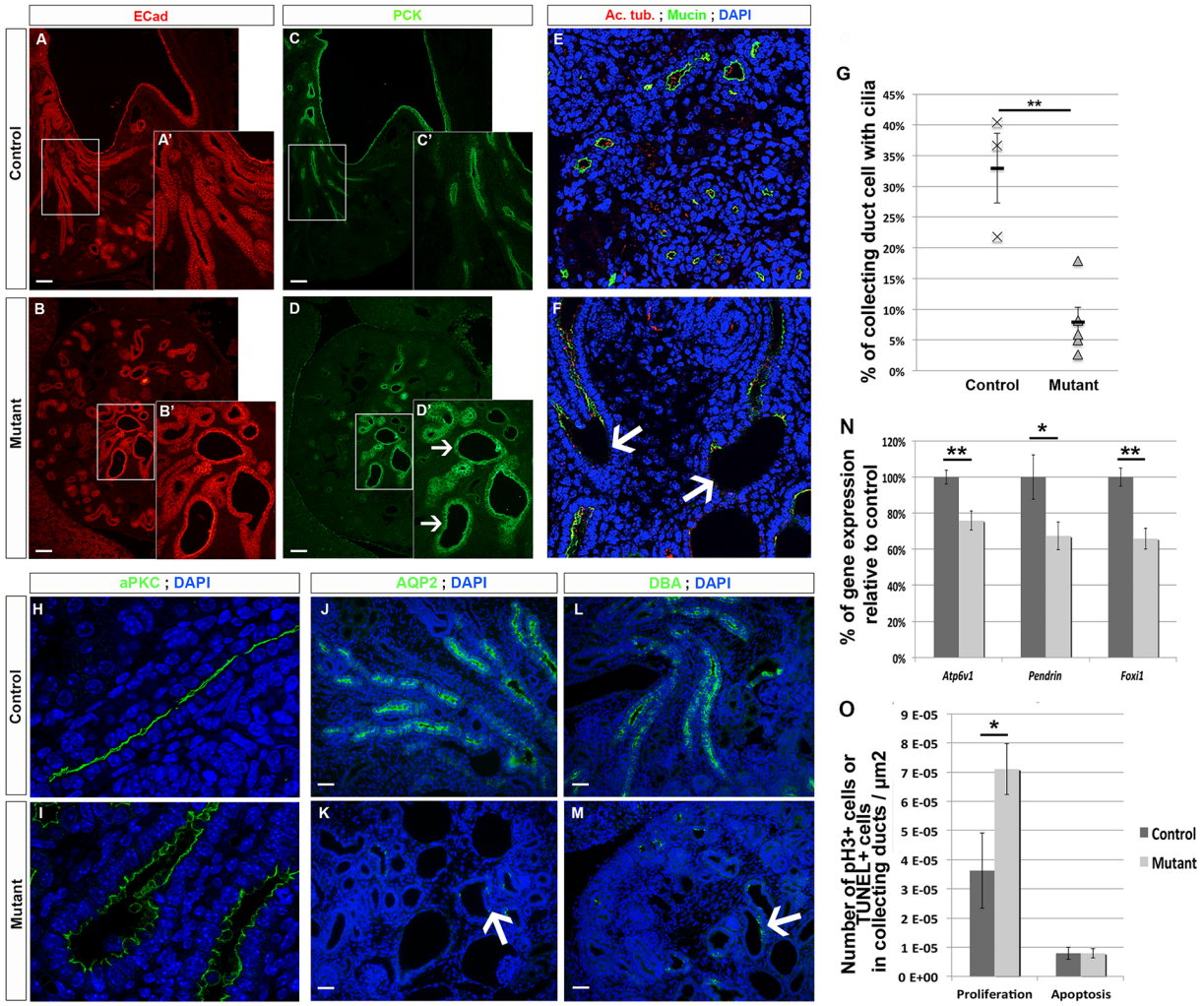

Fig. 8. HNF1B is required for collecting duct cell differentiation. (A-D) Immunohistochemistry of Ecad and PCK at E17.5 shows the formation of cysts (white arrows) in mutant collecting ducts. Scale bars: 100 µm. (E,F) co-staining of mucin and acetylated tubulin shows loss of the apical mucin staining and primary cilia in developing mutant cysts (white arrows). (G) Quantification of cilia number in collecting ducts shows a 25% decrease in mutant kidneys compared with control. $^{**}P<0.01$; data are mean±s.e.m. (H,I) Immunohistochemistry of aPKC shows disorganization of the apical staining in mutant collecting ducts. (J-M) Immunostaining for the principal cell markers AQP2 (J,K) and DBA (L,M) at E17.5. White arrows indicate very few stained cells in mutant kidneys. Scale bars: 40 µm. (N) qRT-PCR of principal (*Atp6v1*) and intercalated cell markers (*Foxi1* and pendrin) shows defective differentiation of E17.5 collecting ducts. *n*=6 controls and 6 mutants (*n* being a pool of the two embryo kidneys). (O) (Left) Quantification of pH3-positive cells in E17.5 collecting ducts indicates an increase in proliferation in mutants. (Right) Quantification of TUNEL signal in E17.5 collecting ducts shows no difference in apoptosis levels between controls and mutants. $^{*}P<0.05$, $^{**}P<0.01$; data are mean±s.e.m.

Gfra1 is a Ret co-receptor and Etv5 a downstream effector. An early role of *Gfra1* in UB induction has been established (Keefe Davis et al., 2013). Although these two genes have individually limited impact on branching morphogenesis after UB induction (Keefe Davis et al., 2013; Lu et al., 2009), we can hypothesize that combined downregulation of *Gfra1* and *Etv5* contribute to the defective maintenance of the GDNF/Ret signaling. In addition, *Hnf1b*-mutant cells exhibit abnormal cell-cell contacts and basal membrane in UB tips. Interestingly abnormal cell-cell contacts have also been reported in *Mek1/2* mutants (Ihermann-Hella et al., 2014), further supporting the requirement of HNF1B for the maintenance of the GDNF/Ret pathway. In addition, *Hnf1b* mutant cells show defective apicobasal polarity and cell-cell adhesion in nascent trunks. This may suggest that HNF1B has a more-general role in epithelial cell polarity than merely regulating RET signaling. Moreover, in contrast to $Ret^{-/-}$ cells, but similar to *Etv4/5* mutant cells, *Hnf1b* mutant cells (Kuure et al., 2010) were not excluded from the common nephric duct (data not shown). We can therefore ask whether HNF1B acts either sequentially or in parallel to maintain epithelial organization and GDNF/Ret signaling.

Interestingly, in our mutants, Pax2 is virtually absent in the mutant UB branches and CDs, and previous studies have shown that decreased levels of *Pax2* in the $Pax2^{Neu/+}$ heterozygous mutants is associated with reduced branching (Porteous et al., 2000). Although the precise role of Pax2 in branching has not been directly addressed in the ureteric cell lineage, it has been shown that in addition to its role in *Gdnf* induction in the MM, *Pax2* has an intrinsic function in UB branching (Brophy et al., 2001). It has also been shown that *Ret* in the developing kidney is responsive to *Pax2* gene dose (Clarke et al., 2006). Moreover, the analysis of a recently generated hypomorphic allele of *Pax2* indicates the crucial role of this transcription factor in maintaining epithelial polarity of the nephric duct. Interestingly, the *Pax2* hypomorphic phenotype exhibited, in addition to hypoplasia, duplicated ureters, cystic kidneys and fewer nephrons (Soofi et al., 2012), thus sharing several of the phenotypes observed in our mutants.

Development (2017) 144, 4704-4719 doi:10.1242/dev.154336

UB-tip cells display a specific proliferation mode, morphology and gene expression pattern (Schmidt-Ott et al., 2005; Yu et al., 2012). Tip cells are also progenitor cells: while one part of the pool remains at the tip to create new branches, the other part is left in the trunk to differentiate into CDs (Shakya et al., 2005). MACD may be one of the processes underlying this asymmetric cell division of progenitor cells. Analysis of our data suggested that the defective dispersal of mutant daughter cells during MACD could contribute to the UB branching defect. However, MACD contributes to relatively short-range cell movements and clonal analysis has recently shown that many cell rearrangements occur between cell divisions (Chi et al., 2009a). Moreover, although *Ret* signaling does promote directed cell movements in the UB tips, it apparently has no effect on MACD (Riccio et al., 2016). Although the developmental consequences of altered MACD remain to be elucidated, we can speculate that the loss of apicobasal polarity could be contributing to the cell dispersal defect observed in our mutants. Furthermore, most cells do not move as isolated entities *in vivo* but interact with their neighbors during migration (Ghabrial and Krasnow, 2006; Ewald et al., 2008). Our results also show the importance of the neighboring cells during MACD for cell movements, suggesting that this process relies on cell-cell interactions. It is possible that interactions among the mutant cells are impaired in the UB, thereby leading to reduced branching.

We found that the degree of mosaicism is directly linked to the severity of the phenotype both *in vivo* and *in vitro* as cultured UBs with few GFP^{-} cells did not develop any further branching after the 'T' shape stage. It is interesting to note that in *Hnf1b-Sox2-Cre* mutants and the previously described tetraploid chimeras, branching stops after the 'T'-stage (Lokmane et al., 2010).

A later role for HNF1B in proper collecting duct morphogenesis and epithelial lumen formation

Owing to the mosaicism of the *HoxB7-Cre* line, a sufficient amount of wild-type cells was present to enable continued branching after the 'T'-stage. OPT analysis showed that specific branching parameters were also severely affected. This defective UB architecture disrupts the cortico-medullary axis of the kidneys and affects the number and organization of developing nephrons and is very likely to be responsible for the observed perinatal lethality.

Late-stage embryos or P0 mutants exhibit severe urogenital abnormalities reminiscent of CAKUT. Interestingly, heterozygous mutations in the human *HNF1B* gene are the most common cause of monogenic CAKUT and account for 5 to 31% of cases, depending on the cohort examined (Raaijmakers et al., 2015). Mutant CDS also exhibit abnormal localization of apical markers and disruption of tissue architecture, leading to cystic dilatations. Our results demonstrate that HNF1B controls the expression of several genes that exhibit apico-basal polarity, such as *Atp6v1b1*, *Slc26a4*, *Pdzk1*, *Aqp5*, *Hpn* and *Tmem27* (Table S2).

Previous studies in postnatal cystic kidneys, upon *Hnf1b* inactivation in medullar renal tubules, reported reduced expression of genes involved in cystogenesis, including *Pkd2*, *Pkhd1*, *Nphp1*, *Tg737/polaris* (*Ift88*) and *Umod* (Gresh et al., 2004), thus potentially linking the HNF1B transcriptional regulatory cascade to ciliogenesis. However, this expression analysis was performed in severe postnatal cystic kidneys. In our mRNA-seq analysis *Pkd2*, *Nphp1* and *Tg737/polaris* were not downregulated in mutants. Moreover, other known HNF1B targets, such as *Pkhd1* (Gresh et al., 2004; Hiesberger et al., 2005) and *Cys1* (De Vas et al., 2015) were downregulated in our mutants, but under the cutoff value. More importantly, the cystic phenotypes of either *Pkdh1* or *Cys^{cpk}* mutant mice do not phenocopy that observed in our mutants. *Pkhd1* mutants had normal kidney morphology at birth and renal cysts were first detected postnatally (45 days of age) (Williams et al., 2008). Similarly, *Cys^{cpk}* mouse developed cysts only postnatally, initially in the proximal tubules and subsequently by P15 in the collecting ducts (Ricker et al., 2000). Notably, we found that CDs are either dilated or develop cysts from around E16. Similar developmental phenotypes have been observed in the context of the RCAD pathology in human fetuses (Chen et al., 2010), and increasing amounts of data report renal developmental abnormalities during gestation (Clissold et al., 2015). Thus, although reduced expression of *Pkhd1* and *Cys1* may contribute to some aspects of renal phenotype, the mechanisms of cyst formation are not simply explained by downregulation of these genes.

In our mutants, defects in epithelial organization and polarity precede cyst initiation. Moreover, non-dilated tubules contained apparently structurally normal cilia, thus suggesting that HNF1B does not regulate the expression of an essential structural component of cilia. However, cystic tubules contained fewer cells with primary cilia, suggesting that loss of cilia may be secondary to the loss of apicobasal polarity or due to increased proliferation.

The RNA-seq analysis shows upregulation of genes encoding cytoskeleton proteins and a downregulation of membranous genes, encoding protein components of the cell membrane and cell-cell junctions. Interestingly, similar defects have been observed in cell-cell junction mutants in other branching organs (Plosa et al., 2014; Shih et al., 2016). Remarkably, several of the most downregulated genes in mutants are associated with abnormal collecting duct epithelium, ureter morphology and pelvic urothelium differentiation, as well as hydronephrosis. Our study also shows that these deregulations can be both direct and indirect, as in our E14.5 ChIP-seq data HNF1B was found to be recruited on consensus binding sites in the promoter/enhancer regions of several genes (C.H. and S.C., unpublished; Table S1). Of interest is the identification, among the most downregulated genes, of novel HNF1B putative target genes, notably *Foxa1*, *Esrrg*, *Lgals3*, *Kcnj1*, *Kcnj16*, *Atp6v0a4* and *Cldn19*, which can be associated with several of the pathogenic characteristics of the RCAD disease (Bullock et al., 2001; Chiu et al., 2006; Lee et al., 2006; Yan et al., 2008; Berry et al., 2011; Paulais et al., 2011; Norgett et al., 2012). In particular, our data uncover an unappreciated role of HNF1B in renal and pelvic urothelium differentiation, likely via the transcriptional control of Foxa1, which in turn regulates uroplakin genes (Varley et al., 2009; Yu et al., 2012). These findings are therefore expected to provide a deeper understanding of the complex syndrome RCAD and be a valuable resource to orientate further investigations.

In conclusion, our results show that HNF1B is an essential transcriptional regulator required for UB branching, morphogenesis and patterning. It seems to be required cell-autonomously for the acquisition of a specialized UB-tip domain, at least in part, through the establishment and maintenance of cell-cell adhesion, as well as *Pax2* expression and the maintenance of *Ret* signaling. HNF1B is subsequently required in the trunk for the establishment of normal apicobasal polarity and tubular organization.

MATERIALS AND METHODS

Mouse transgenic lines and crossing strategies

Hnf1b-null (*Hnf1b$^{lacZ/+}$*) mice in which the *lacZ* gene replaced the first exon (Barbacci et al., 1999) and *HoxB7-Cre* (Yu et al., 2002) or *Sox2-Cre* (Hayashi et al., 2002) transgenic mice were kept as heterozygotes. The *Hnf1b* conditional knockout (*Hnf1b$^{Flox/Flox}$*) carrying LoxP sites flanking exon 4 was as previously described (Heliot et al., 2013). The R26RYFP line

Development (2017) 144, 4704-4719 doi:10.1242/dev.154336

[B6.129X1-Gt (ROSA)26Sor$^{tm1(EYFP)Cos}$/J] was from Jackson Laboratory. (ROSA)26Sor$^{tm4(ACTB-tdTomato,-EGFP)Luo}$/J (R26-mT/mG) reporter mice and *Hnf1b$^{Flox/Flox}$* mice were kept as double homozygous.

HoxB7-Cre;Hnf1b$^{lacZ/+}$ compound heterozygous males and *Hnf1b$^{fl/fl}$* females were crossed to generate *HoxB7-Cre;Hnf1b$^{lacZ/fl}$* embryos and were referred to as mutants. *Hnf1b$^{lacZ/fl}$* and *Hnf1b$^{+/fl}$* embryos that lacked the *HoxB7-Cre* transgene were referred to as controls, due to the lack of a phenotype in heterozygous embryos for the *Hnf1b-lacZ-null* allele (Barbacci et al., 1999; Kornfeld et al., 2013). *HoxB7-Cre;Hnf1b$^{+/fl}$* embryos were referred to as heterozygous and showed no phenotype (Fig. S1).

ROSA26$^{loxP\text{-}mtomato\text{-}loxP\text{-}mEGFP}$;Hnf1$^{fl/fl}$ compound homozygous females were crossed with *HoxB7-Cre;Hnf1b$^{lacZ/+}$* males to generate either mutant embryos (*HoxB7$^{Cre/+}$; Hnf1b$^{fl/lacZ}$; ROSA26$^{loxP\text{-}mtomato\text{-}loxP\text{-}mEGFP}$*) or control embryos, lacking the *Hnf1b^{lacz}* null allele (*HoxB7$^{Cre/+}$; Hnf1b$^{fl/+}$; ROSA26$^{loxP\text{-}mtomato\text{-}loxP\text{-}mEGFP}$*). In both control and mutant embryos, the expression of the Cre recombinase deleted the mtomato gene, encoding the membrane-bound tomato protein (mT) and induced the membrane-bound EGFP.

Ethics

All animal experiments described herein were approved by the Ethic commitees of the University Pierre et Marie Curie and the Ministère de l'Education Nationale, de l'Enseignement Superieur et de la Recherche (N° 04811.01).

Organ cultures and time-lapse imaging

E11.5 kidneys were micro-dissected from *HoxB7Cre$^{+/-}$;Hnf1b$^{flox/+}$; R26$^{mT/mG}$* or *HoxB7Cre$^{+/-}$;Hnf1b$^{flox/lacZ}$;R26$^{mT/mG}$* embryos and placed on Transwell plates (Costar 3450, Corning). The tissues were cultured in DMEM GlutaMAX (GibcoBRL) medium supplemented with 10% FBS, 0.5 mM HEPES and 1% penicillin/streptomycin. For imaging of the kidney cultures on the top of the filter (Costantini et al., 2011), standard six-well glass-bottomed plates were used (BD Falcon). The novel organ culture set-up (FiZD) used for time-lapse imaging is described in detail elsewhere (Saarela et al., 2017). The culture plates were inserted into an on-stage incubator on a Zeiss LSM780 confocal microscope at 37°C and 5% CO_2 (OkoLab Bold Line Temperature Controller, Gas Controller, cage enclosure and top stage incubator). Time-lapse images of the kidney explants were captured at 5 to 10 min intervals and processed with the Zen Blue program (2012, Zeiss). Huygens Professional (Scientific Volume Imaging) was used for *z*-stack deconvolution and pictures were prepared using Imaris (Bitplane) or Fiji (Schindelin et al., 2012).

Proliferation rate quantification and cell tracking

Mitotic GFP$^+$ cells are of circular shape with bright boundaries and dark centers; they were detected using multi-scale template matching. Templates were learnt from a few manually marked mitotic cells. Detections persisting at the same location in multiple consecutive frames were filtered and only the last among them was retained. The number of cells in a frame was estimated using the kidney volume and average cell size in that frame. The volume of kidney was computed by segmenting it using thresholding followed by morphological filtering and the average cell size in a frame was estimated from the mean size of detected mitotic cells. Manually annotated cell (only mitotic and daughter) markers were used to guide the segmentation. Hessian ridge enhancement (Hodneland et al., 2013) was used to remove small bright regions inside cell bodies and enhance the signal at cell membrane to fill small gaps. Cell centroids from cell segmentation were used to measure the distance of daughter cells from the site of mitosis and from each other. The proportion of shared border between a daughter pair was computed by normalizing the number of pixels where both daughter cells were in contact with the perimeter of the smallest daughter cell. If both daughters touched each other at a time point, they were counted as an in-contact pair.

Histology, immunostaining and TUNEL

Kidneys from embryos/newborns were fixed, embedded in paraffin wax, sectioned and then stained with Hematoxylin and Eosin or antibodies as described previously (Lokmane et al., 2008). We used rabbit anti-HNF1B (Santa Cruz Biotechnology, H-85, sc-22840; 1:100), chicken anti-GFP (Aves Labs, GFP-1020; 1:300) (GFP antibody was used to detect YFP as they share GFP epitope antibody recognition), biotinylated LTA (Vector Laboratory, B-1325; 1:100), rabbit anti-NKCC2 (Biosciences, SPC-401D; 1:200), rabbit anti-AQP2 (kindly provided by M. Knepper, NIH, Bethesda, USA), rabbit anti-PAX2 (Covance, PRB-276P; 1:200), rabbit anti-AQP1 (Interchim, Alpha Diagnostic, AQP11-A; 1:200), rabbit anti-aPKCz (Santa Cruz, C-20, sc-216; 1:50), biotinylated DBA (Vector Laboratory, B-1035; 1:100), mouse anti-β-catenin (BD Transduction Laboratories, 610153; 1:100), rabbit anti-phosphoHistone H3 (Upstate Cell Signaling, 06-570; 1:200), rabbit anti-WT1 (Santa Cruz Biotechnology, C-19, sc-192; 1:100), rabbit anti-Laminin (Sigma-Aldrich, L-9393; 1:100), mouse anti-E-cadherin (BD Transduction Laboratories, 610182; 1:50), mouse anti-pan-cytokeratin (Sigma-Aldrich, C1801; 1:200), Armenian hamster anti-MUC1 (Neomarkers, HM-1630-P1; 1:100), mouse anti-acetylated alpha-tubulin (Sigma-Aldrich, T6557; 1:100) and rabbit anti-Wnt11 (GeneTex, GTX105971; 1:100). Staining of kidney culture was performed after 5 days of culture. After fixation in 4% paraformaldehyde (PFA), permeabilization with PBS+0.5% Triton X-100 and blocking with 5% fetal bovine serum (FBS) in DMSO, we used rat anti-Troma-1 (developed by R. Kemler and obtained from DSHB; 1:500) and rabbit anti-Laminin (Sigma-Aldrich, L9393; 1:500) as primary antibodies. Terminal deoxynucleotidyltransferase-mediated dUTPbiotin nick end-labeling (TUNEL) was performed as described previously (Paces-Fessy et al., 2012).

In situ hybridization

In situ hybridization on paraffin sections were performed as described previously (Lokmane et al., 2008).

Optical projection tomography

Whole-mount E13.5 (n=10 controls and 6 mutants) and E16 (n=6 controls and 6 mutants) kidneys were fixed in 4% paraformaldehyde (PFA) and processed for optical projection tomography (OPT) as described previously with some modifications (Chi et al., 2011). Fixed kidneys were stained with rat anti-Troma-1 (DSHB; 1:500) and anti-Ezrin antibodies (a kind gift from Monique Arpin and Sylvie Robine, Institut Curie, Paris, France) at 4°C for 2 days and then extensively washed in TBST (Tris-buffered saline with 0.01% Triton X-100 and 10% FBS). Secondary antibodies were applied at 4°C for 2 days followed by several washes in TBST. Samples were embedded in 1% low melting point agarose. Agarose blocks were placed in absolute methanol and cleared with benzyl alcohol/benzyl benzoate solution (1:2); images were captured using a 3001 OPT scanner (Bioptonics Microscopy). Pictures were prepared using Imaris (Bitplane) and morphometric parameters were calculated using Tree Surveyor Software (Short et al., 2013).

Quantitative reverse transcription PCR and chromatin immunoprecipitation assays

Total RNA extraction from embryonic kidneys, reverse transcription and qPCR were performed as described previously (Paces-Fessy et al., 2012). Number of kidney samples is indicated in figure legends. The following primers were used (forward/reverse): cyclophilin A, CAGGTCCTGGCATCTTGTCC/TTGCTGGTCTTGCCATTCCT; *Hnf1b* wild-type, GGCCTACGACCGGCAAAAGA/GGGAGACCCCTCGTTGCAAA; *Ret*, ACACCTTCGGACTCACTGCT/CAGGGGTGTCTCCTCTTCTG; *Gfra1*, CTTCGTGCTGCCACTCCTGG/CTCAGTGTGCGGTACTTGGTG; *Etv5*, CGTTTGATCTTGGTTGGAGG/GCTGAAGCACAAGTTCCTGA; *Wnt11*, GCAGTGCAACAAGACTTCCA/TCCACCACTCTGTCCGTGTA; *Wnt9b*, CGAGGAGATGCGAGAGTGC/GGAAGGGTGTCAGGACCTC; *Pax2*, GGGCATCTGCGATAATGACA/GGTCCGGATGATCCTGTTGAT; *Cdh16*, GTCCCCACCATCCCTTACAA/CTCCCTCCTTCAAACCGAGT; *Pkhd1*, TGCTCCTCAGGCAGGCAATCG/ACCTGTACCCTGGGGTGGCTT; *Cys1*, AGAGGAGCTCATGGCGAGCATT/GCCTGTGGCACAGATGCCAAGA; *Foxi1*, TCCCATGGCTACTGAGGTTG/CCTCTCCACCATGACAGCAT; *Atp6v1*, CCCTGAAGTCCCTTCAAACA/TGGACCAGGTCAAGTTTGC; and pendrin, GGAACTGCAGCTAGTAGGGC/CCCAAATACCGAGTCAAGGA.

Development (2017) 144, 4704-4719 doi:10.1242/dev.154336

Chromatin immunoprecipitation (ChIP) was performed on E14.5 kidneys using the rabbit HNF1B antibody (H85, Santa Cruz) as described by Heliot and Cereghini (2012). Each ChIP was validated by assaying the two well-known HNF1B targets genes Ksp-cadherin and Wnt9 (first intron) and a negative control (Heliot and Cereghini, 2012; Heliot et al., 2013; Lokmane et al., 2010) (data not shown). The following primers were used (forward/reverse): *Gfra1*, GAACCCCTGTCTTGGGCCT/AACCCGCATGGCTCT-GTG; and *Etv5*, TTTTTCCACAGGCTGCACAAT/GGGCCCACTGGC-AGACTT.

Electron microscopy

E15 control (n=2) and mutant (n=2) kidneys were dissected cut into quarters and fixed in fresh 1% glutaraldehyde/4% PFA in 0.1 M PBS. Sample processing was carried out using the Tecnai GS Spirit Bio Twin microscope (FEI Europe) and the images were captured with a Quemesa CCD camera controlled by the iTEM software (Olympus Soft Imaging Solutions).

RNA sequencing

RNA was extracted from E15.5 kidneys, two controls and two mutant embryos (four kidneys of each genotype in total) from the same litter. The raw bam files, one for each RNA-seq sample, were summarized to a gene read counts table, using the Bioconductor open source software package GenomicRanges. In the final read counts table, each row represents one gene; each column represents one RNA-seq sample; and each cell represents the corresponding read counts associated with each row and column. The gene counts table was normalized for inherent systematic or experimental biases (e.g. sequencing depth, gene length, GC content bias) using the Bioconductor package edgeR after removing genes that had zero counts over all RNA-seq samples (Moulos and Hatzis, 2015). Functional enrichment gene lists were established with ToppGene suite (Chen et al., 2009).

Statistical analysis

For comparison of several means, normality of the variables was checked and we performed Student's t-tests with a confidence interval of 95%. *P<0.05; **P<0.01 ***P<0.001; error bars indicate s.e.m.

Acknowledgements

We thank Marie Breau and Daniel Darby for critical reading of the manuscript; Paula Haipus for technical assistance in kidney organ culture; and Eduard Manzoni and Edwige Declercq for animal care. We thank Pantelis Hatzis and Martin Reczko (Alexander Fleming Institute, Genomics Facility, Greece) for mRNA sequencing. We also thank Sylvie Schneider-Maunoury (UMR7622 CNRS-UPMC) for support to complete this study. The anti-Troma-1 antibody was obtained from the Developmental Studies Hybridoma Bank (DSHB), which was created by the NICHD of the NIH at The University of Iowa, Department of Biology, Iowa, USA.

Competing interests

The authors declare no competing or financial interests.

Author contributions

Conceptualization: A.D., S.C.; Methodology: A.D., C.H., I.S., V.-P.R., S.C.; Validation: A.D., S.C.; Formal analysis & Software: S.U.A., J.H.; Visualization: A.D.; Investigation: A.D., C.H., I.S., I.M., S.C.; Writing – original draft preparation: A.D., S.C.; Review-Editing: all authors; Resource and Funding acquisition: S.C., S.J.V., Supervision: S.C.; Project administration: S.C.

Funding

This work was supported by the Institut National de la Santé et de la Recherche Médicale (INSERM, France); by the European Community Seventh Framework Programme FP7/2009 - Marie Curie Initial Training Network (ITN) Project BOLD 238821; by the Centre National de la Recherche Scientifique (CNRS, France); by the Université Pierre et Marie Curie (to S.C.); by the Suomen Akatemia (206038, 121647, 250900 and 260056) and a Centre of Excellence grant 2012–2017 from the Suomen Akatemia (251314); and by the Sigrid Jusélius Stiftelse and European Community's Seventh Framework Programme FP7/2009 (305608; EURenOmics: European Consortium for High-Throughput Research in Rare Kidney Diseases to S.J.V.). A.D. was supported by a PhD student fellowship from the Ministère de l'Enseignement Supérieur, de la Recherche Scientifique et des Technologies de l'Information et de la Communication and by a long-term fellowship from the European Renal Association – European Dialysis and Transplant Association (ERA-EDTA LTF-STF: 177-2014).

Data availability

RNA-seq data are deposited at Gene Expression Omnibus (GSE106085).

Supplementary information

Supplementary information available online at
http://dev.biologists.org/lookup/doi/10.1242/dev.154336.supplemental

References

Bai, Y., Pontoglio, M., Hiesberger, T., Sinclair, A. M. and Igarashi, P. (1995). Regulation of kidney-specific Ksp-cadherin gene promoter by hepatocyte nuclear factor-1beta. *Am. J. Physiol. Renal. Physiol.* **283**, F839-F851.

Barbacci, E., Reber, M., Ott, M., Breillat, C., Huetz, F. and Cereghini, S. (1999). Variant hepatocyte nuclear factor 1 is required for visceral endoderm specification. *Development* **126**, 4795-4805.

Barbacci, E., Chalkiadaki, A., Masdeu, C., Haumaitre, C., Lokmane, L., Loirat, C., Cloarec, S., Talianidis, I., Bellanné-Chantelot, C. and Cereghini, S. (2004). HNF1beta/TCF2 mutations impair transactivation potential through altered co-regulator recruitment. *Hum. Mol. Genet.* **13**, 3139-3149.

Bellanné-Chantelot, C., Chauveau, D., Gautier, J.-F., Dubois-Laforgue, D., Clauin, S., Beaufils, S., Wilhelm, J.-M., Boitard, C., Noël, L.-H., Velho, G. et al. (2004). Clinical spectrum associated with hepatocyte nuclear factor-1beta mutations. *Ann. Intern. Med.* **140**, 510-517.

Berry, R., Harewood, L., Pei, L., Fisher, M., Brownstein, D., Ross, A., Alaynick, W. A., Moss, J., Hastie, N. D., Hohenstein, P. et al. (2011). Esrrg functions in early branch generation of the ureteric bud and is essential for normal development of the renal papilla. *Hum. Mol. Genet.* **20**, 917-926.

Bohn, S., Thomas, H., Turan, G., Ellard, S., Bingham, C., Hattersley, A. T. and Ryffel, G. U. (2003). Distinct molecular and morphogenetic properties of mutations in the human HNF1beta gene that lead to defective kidney development. *J. Am. Soc. Nephrol.* **14**, 2033-2041.

Brophy, P. D., Ostrom, L., Lang, K. M. and Dressler, G. R. (2001). Regulation of ureteric bud outgrowth by Pax2-dependent activation of the glial derived neurotrophic factor gene. *Development* **128**, 4747-4756.

Bullock, S. L., Johnson, T. M., Bao, Q., Hughes, R. C., Winyard, P. J. and Woolf, A. S. (2001). Galectin-3 modulates ureteric bud branching in organ culture of the developing mouse kidney. *J. Am. Soc. Nephrol.* **12**, 515-523.

Chen, J., Bardes, E. E., Aronow, B. J. and Jegga, A. G. (2009). ToppGene Suite for gene list enrichment analysis and candidate gene prioritization. *Nucleic Acids Res.* **37**, W305-W311.

Chen, Y. Z., Gao, Q., Zhao, X. Z., Chen, Y. Z., Bennett, C. L., Xiong, X. S., Mei, C. L., Shi, Y. Q. and Chen, X. M. (2010). Systematic review of TCF2 anomalies in renal cysts and diabetes syndrome/maturity onset diabetes of the young type 5. *Chin. Med. J.* **123**, 3326-3333.

Chi, X., Hadjantonakis, A.-K., Wu, Z., Hyink, D. and Costantini, F. (2009a). A transgenic mouse that reveals cell shape and arrangement during ureteric bud branching. *Genesis* **47**, 61-66.

Chi, X., Michos, O., Shakya, R., Riccio, P., Enomoto, H., Licht, J. D., Asai, N., Takahashi, M., Ohgami, N., Kato, M. et al. (2009b). Ret-dependent cell rearrangements in the Wolffian duct epithelium initiate ureteric bud morphogenesis. *Dev. Cell* **17**, 199-209.

Chi, L., Saarela, U., Railo, A., Prunskaite-Hyyryläinen, R., Skovorodkin, I., Anthony, S., Katsu, K., Liu, Y., Shan, J., Salgueiro, A. M. et al. (2011). A secreted BMP antagonist, Cer1, fine tunes the spatial organization of the ureteric bud tree during mouse kidney development. *PLoS ONE* **6**, e27676.

Chiu, M. G., Johnson, T. M., Woolf, A. S., Dahm-Vicker, E. M., Long, D. A., Guay-Woodford, L., Hillman, K. A., Bawumia, S., Venner, K., Hughes, R. C. et al. (2006). Galectin-3 associates with the primary cilium and modulates cyst growth in congenital polycystic kidney disease. *Am. J. Pathol.* **169**, 1925-1938.

Clarke, J. C., Patel, S. R., Raymond, R. M., Jr, Andrew, S., Robinson, B. G., Dressler, G. R. and Brophy, P. D. (2006). Regulation of *c-Ret* in the developing kidney is responsive to *Pax2* gene dosage. *Hum. Mol. Genet.* **15**, 3420-3428.

Clissold, R. L., Hamilton, A. J., Hattersley, A. T., Ellard, S. and Bingham, C. (2015). HNF1B-associated renal and extra-renal disease-an expanding clinical spectrum. *Nat. Rev. Nephrol.* **11**, 102-112.

Coffinier, C., Gresh, L., Fiette, L., Tronche, F., Schutz, G., Babinet, C., Pontoglio, M., Yaniv, M. and Barra, J. (2002). Bile system morphogenesis defects and liver dysfunction upon targeted deletion of HNF1beta. *Development* **129**, 1829-1838.

Costantini, F. (2012). Genetic controls and cellular behaviors in branching morphogenesis of the renal collecting system. *Wiley Interdiscip. Rev. Dev. Biol.* **1**, 693-713.

Costantini, F., Watanabe, B., Lu, B., Chi, X. and Srinivas, S. (2011). Dissection of embryonic mouse kidney, culture in vitro, and imaging of the developing organ. *Cold Spring Harb. Protoc.* **5**, pdb.prot5613.

De Vas, M. G., Kopp, J. L., Heliot, C., Sander, M., Cereghini, S. and Haumaitre, C. (2015). Hnf1b controls pancreas morphogenesis and the generation of Ngn3+ endocrine progenitors. *Development* **142**, 871-882.

Ewald, A. J., Brenot, A., Duong, M., Chan, B. S. and Werb, Z. (2008). Collective epithelial migration and cell rearrangements drive mammary branching morphogenesis. *Dev. Cell* **14**, 570-581.
Ghabrial, A. S. and Krasnow, M. A. (2006). Social interactions among epithelial cells during tracheal branching morphogenesis. *Nature* **441**, 746-749.
Gjorevski, N. and Nelson, C. M. (2010). Branch formation during organ development. *Wiley Interdiscip. Rev. Dev. Biol.* **2**, 734-741.
Gresh, L., Fischer, E., Reimann, A., Tanguy, M., Garbay, S., Shao, X., Hiesberger, T., Fiette, L., Igarashi, P., Yaniv, M. et al. (2004). A transcriptional network in polycystic kidney disease. *EMBO J.* **23**, 1557-1568.
Haumaitre, C., Barbacci, E., Jenny, M., Ott, M. O., Gradwohl, G. and Cereghini, S. (2005). Lack of TCF2/vHNF1 in mice leads to pancreas agenesis. *Proc. Natl. Acad. Sci. USA* **102**, 1490-1495.
Haumaitre, C., Fabre, M., Cormier, S., Baumann, C., Delezoide, A.-L. and Cereghini, S. (2006). Severe pancreas hypoplasia and multicystic renal dysplasia in two human fetuses carrying novel HNF1beta/MODY5 mutations. *Hum. Mol. Genet.* **15**, 2363-2375.
Hayashi, S., Lewis, P., Pevny, L. and McMahon, A. P. (2002). Efficient gene modulation in mouse epiblast using a Sox2Cre transgenic mouse strain. *Mech. Dev.* **119**, S97-S101.
Heidet, L., Decramer, S., Pawtowski, A., Morinière, V., Bandin, F., Knebelmann, B., Lebre, A. S., Faguer, S., Guigonis, V., Antignac, C. et al. (2010). Spectrum of HNF1B mutations in a large cohort of patients who harbor renal diseases. *Clin. J. Am. Soc. Nephrol.* **5**, 1079-1090.
Heliot, C. and Cereghini, S. (2012). Analysis of in vivo transcription factor recruitment by chromatin immunoprecipitation of mouse embryonic kidney. *Methods Mol. Biol.* **886**, 275-291.
Heliot, C., Desgrange, A., Buisson, I., Prunskaite-Hyyryläinen, R., Shan, J., Vainio, S., Umbhauer, M. and Cereghini, S. (2013). HNF1B controls proximal-intermediate nephron segment identity in vertebrates by regulating Notch signalling components and Irx1/2. *Development* **140**, 873-885.
Hiesberger, T., Shao, X., Gourley, E., Reimann, A., Pontoglio, M. and Igarashi, P. (2005). Role of the hepatocyte nuclear factor-1beta (HNF-1beta) C-terminal domain in Pkhd1 (ARPKD) gene transcription and renal cystogenesis. *J. Biol. Chem.* **280**, 10578-10586.
Hodneland, E., Kogel, T., Frei, D. M., Gerdes, H.-H. and Lundervold, A. (2013). CellSegm - a MATLAB toolbox for high-throughput 3D cell segmentation. *Source Code Biol. Med.* **8**, 16.
Ihermann-Hella, A., Lume, M., Miinalainen, I. J., Pirttiniemi, A., Gui, Y., Peränen, J., Charron, J., Saarma, M., Costantini, F. and Kuure, S. (2014). Mitogen-activated protein kinase (MAPK) pathway regulates branching by remodeling epithelial cell adhesion. *PLoS Genet.* **10**, e1004193.
Keefe Davis, T., Hoshi, M. and Jain, S. (2013). Stage specific requirement of Gfrα1 in the ureteric epithelium during kidney development. *Mech. Dev.* **130**, 506-518.
Kim, H. Y. and Nelson, C. M. (2012). Extracellular matrix and cytoskeletal dynamics during branching morphogenesis. *Organogenesis* **8**, 56-64.
Kornfeld, J. W., Baitzel, C., Könner, A. C., Nicholls, H. T., Vogt, M. C., Herrmanns, K., Scheja, L., Haumaitre, C., Wolf, A. M., Knippschild, U. et al. (2013). Obesity-induced overexpression of miR-802 impairs glucose metabolism through silencing of Hnf1b. *Nature* **494**, 111-115.
Kuure, S., Cebrian, C., Machingo, Q., Lu, B. C., Chi, X., Hyink, D., D'Agati, V., Gurniak, C., Witke, W. and Costantini, F. (2010). Actin depolymerizing factors cofilin1 and destrin are required for ureteric bud branching morphogenesis. *PLoS Genet.* **6**, e1001176.
Leclerc, K. and Costantini, F. (2016). Mosaic analysis of cell rearrangements during ureteric bud branching in dissociated/reaggregated kidney cultures and in vivo. *Dev. Dyn.* **245**, 483-496.
Lee, N. P. Y., Tong, M. K., Leung, P. P., Chan, V. W., Leung, S., Tam, P.-C., Chan, K.-W., Lee, K.-F., Yeung, W. S. B. and Luk, J. M. (2006). Kidney claudin-19: localization in distal tubules and collecting ducts and dysregulation in polycystic renal disease. *FEBS Lett.* **580**, 923-931.
Lokmane, L., Haumaitre, C., Garcia-Villalba, P., Anselme, I., Schneider-Maunoury, S. and Cereghini, S. (2008). Crucial role of vHNF1 in vertebrate hepatic specification. *Development* **135**, 2777-2786.
Lokmane, L., Heliot, C., Garcia-Villalba, P., Fabre, M. and Cereghini, S. (2010). vHNF1 functions in distinct regulatory circuits to control ureteric bud branching and early nephrogenesis. *Development* **137**, 347-357.
Lu, B. C., Cebrian, C., Chi, X., Kuure, S., Kuo, R., Bates, C. M., Arber, S., Hassell, J., MacNeil, L., Hoshi, M. et al. (2009). Etv4 and Etv5 are required downstream of GDNF and Ret for kidney branching morphogenesis. *Nat. Genet.* **41**, 1295-1302.
Majumdar, A., Vainio, S., Kispert, A., McMahon, J. and McMahon, A. P. (2003). Wnt11 and Ret/Gdnf pathways cooperate in regulating ureteric branching during metanephric kidney development. *Development* **130**, 3175-3185.
Massa, F., Garbay, S., Bouvier, R., Sugitani, Y., Noda, T., Gubler, M.-C., Heidet, L., Pontoglio, M. and Fischer, E. (2013). Hepatocyte nuclear factor 1β controls nephron tubular development. *Development* **140**, 886-896.
Michael, L. and Davies, J. A. (2004). Pattern and regulation of cell proliferation during murine ureteric bud development. *J. Anat.* **204**, 241-255.
Moulos, P. and Hatzis, P. (2015). Systematic integration of RNA-Seq statistical algorithms for accurate detection of differential gene expression patterns. *Nucleic Acids Res.* **43**, e25.
Naylor, R. W., Przepiorski, A., Ren, Q., Yu, J. and Davidson, A. J. (2012). HNF1B is essential for nephron segmentation during Nephrogenesis. *J. Am. Soc. Nephrol.* **24**, 77-87.
Norgett, E. E., Golder, Z. J., Lorente-Cnovas, B., Ingham, N., Steel, K. P. and Karet Frankl, F. E. (2012). Atp6v0a4 knockout mouse is a model of distal renal tubular acidosis with hearing loss, with additional extrarenal phenotype. *Proc. Natl. Acad. Sci. USA* **109**, 13775-13780.
Paces-Fessy, M., Fabre, M., Lesaulnier, C. and Cereghini, S. (2012). Hnf1b and Pax2 cooperate to control different pathways in kidney and ureter morphogenesis. *Hum. Mol. Genet.* **21**, 3143-3155.
Packard, A., Georgas, K., Michos, O., Riccio, P., Cebrian, C., Combes, A. N., Ju, A., Ferrer-Vaquer, A., Hadjantonakis, A.-K., Zong, H. et al. (2013). Luminal mitosis drives epithelial cell dispersal within the branching ureteric bud. *Dev. Cell* **27**, 319-330.
Paulais, M., Bloch-Faure, M., Picard, N., Jacques, T., Ramakrishnan, S. K., Keck, M., Sohet, F., Eladari, D., Houillier, P., Lourdel, S. et al. (2011). Renal phenotype in mice lacking the Kir5.1 (Kcnj16) K+ channel subunit contrasts with that observed in SeSAME/EAST syndrome. *Proc. Natl. Acad. Sci. USA* **108**, 10361-10366.
Plosa, E. J., Young, L. R., Gulleman, P. M., Polosukhin, V. V., Zaynagetdinov, R., Benjamin, J. T., Im, A. M., van der Meer, R., Gleaves, L. A., Bulus, N. et al. (2014). Epithelial β1 integrin is required for lung branching morphogenesis and alveolarization. *Development* **141**, 4751-4762.
Porteous, S., Torban, E., Cho, N. P., Cunliffe, H., Chua, L., McNoe, L., Ward, T., Souza, C., Gus, P., Giugliani, R. et al. (2000). Primary renal hypoplasia in humans and mice with PAX2 mutations: evidence of increased apoptosis in fetal kidneys of Pax2(1Neu) +/- mutant mice. *Hum. Mol. Genet.* **9**, 1-11.
Raaijmakers, A., Corveleyn, A., Devriendt, K., van Tienoven, T. P., Allegaert, K., Van Dyck, M., van den Heuvel, L., Kuypers, D., Claes, K., Mekahli, D. et al. (2015). Criteria for HNF1B analysis in patients with congenital abnormalities of kidney and urinary tract. *Nephrol. Dial. Transplant* **30**, 835-842.
Riccio, P., Cebrian, C., Zong, H., Hippenmeyer, S. and Costantini, F. (2016). Ret and Etv4 promote directed movements of progenitor cells during renal branching morphogenesis. *PLoS Biol.* **14**, e1002382.
Ricker, J. L., Gattone, V. H., II, Calvet, J. P. and Rankin, C. A. (2000). Development of autosomal recessive polycystic kidney disease in BALB/c-cpk/cpk mice. *J. Am. Soc. Nephrol.* **11**, 1837-1847.
Saarela, U., Akram, S. U., Desgrange, A., Rak-Raszewska, A., Shan, J., Cereghini, S., Ronkainen, V.-P., Heikkilä, J., Skovorodkin, I. and Vainio, S. (2017). Novel fixed z-direction (FiZD) kidney primordia and an organoid culture system for time-lapse confocal imaging. *Development* **144**, 1113-1117.
Schindelin, J., Arganda-Carreras, I., Frise, E., Kaynig, V., Longair, M., Pietzsch, T., Preibisch, S., Rueden, C., Saalfeld, S., Schmid, B. et al. (2012). Fiji: an open-source platform for biological-image analysis. *Nat. Methods* **9**, 676-682.
Schmidt-Ott, K. M., Yang, J., Chen, X., Wang, H., Paragas, N., Mori, K., Li, J. Y., Lu, B., Costantini, F., Schiffer, M. et al. (2005). Novel regulators of kidney development from the tips of the ureteric bud. *J. Am. Soc. Nephrol.* **16**, 1993-2002.
Shakya, R., Watanabe, T. and Costantini, F. (2005). The role of GDNF/Ret signaling in ureteric bud cell fate and branching morphogenesis. *Dev. Cell* **8**, 65-74.
Shih, H. P., Panlasigui, D., Cirulli, V. and Sander, M. (2016). ECM signaling regulates collective cellular dynamics to control pancreas branching morphogenesis. *Cell Rep.* **14**, 169-179.
Short, K., Hodson, M. and Smyth, I. (2013). Spatial mapping and quantification of developmental branching morphogenesis. *Development* **140**, 471-478.
Short, K. M., Combes, A. N., Lefevre, J., Ju, A. L., Georgas, K. M., Lamberton, T., Cairncross, O., Rumballe, B. A., McMahon, A. P., Hamilton, N. A. et al. (2014). Global quantification of tissue dynamics in the developing mouse kidney. *Dev. Cell* **29**, 188-202.
Soofi, A., Levitan, I. and Dressler, G. R. (2012). Two novel EGFP insertion alleles reveal unique aspects of Pax2 function in embryonic and adult kidneys. *Dev. Biol.* **365**, 241-250.
Tao, B., Bu, S., Yang, Z., Siroky, B., Kappes, J. C., Kispert, A. and Guay-Woodford, L. M. (2009). Cystin localizes to primary cilia via membrane microdomains and a targeting motif. *J. Am. Soc. Nephrol.* **20**, 2570-2580.
Thomson, R. B. and Aronson, P. S. (1999). Immunolocalization of Ksp-cadherin in the adult and developing rabbit kidney. *Am. J. Physiol.* **277**, F146-F156.
Varley, C. L., Bacon, E. J., Holder, J. C. and Southgate, J. (2009). FOXA1 and IRF-1 intermediary transcriptional regulators of PPARgamma-induced urothelial cytodifferentiation. *Cell Death Differ.* **1**, 103-114.
Verdeguer, F., Le Corre, S., Fischer, E., Callens, C., Garbay, S., Doyen, A., Igarashi, P., Terzi, F. and Pontoglio, M. (2010). A mitotic transcriptional switch in polycystic kidney disease. *Nat. Med.* **16**, 106-110.
Wang, S., Luo, Y., Witman, G. B. and Zhou, J. (2004). The autosomal recessive polycystic kidney disease protein is localized to primary cilia with concentration in the basal body area. *J. Am. Soc. Nephrol.* **15**, 592-602.

Development (2017) 144, 4704-4719 doi:10.1242/dev.154336

Watanabe, T. and Costantini, F. (2004). Real-time analysis of ureteric bud branching morphogenesis in vitro. *Dev. Biol.* **271**, 98-108.

Wild, W., Pogge von Strandmann, E., Nastos, A., Senkel, S., Lingott-Frieg, A., Bulman, M., Bingham, C., Ellard, S., Hattersley, A. T. and Ryffel, G. U. (2000). The mutated human gene encoding hepatocyte nuclear factor 1beta inhibits kidney formation in developing Xenopus embryos. *Proc. Natl. Acad. Sci. USA* **97**, 4695-4700.

Williams, S. S., Cobo-Stark, P., James, L. R., Somlo, S. and Igarashi, P. (2008). Kidney cysts, pancreatic cysts, and biliary disease in a mouse model of autosomal recessive polycystic kidney disease. *Pediatr. Nephrol.* **23**, 733-741.

Wilson, P. D. (2011). Apico-basal polarity in polycystic kidney disease epithelia. *Biochim. Biophys. Acta* **1812**, 1239-1248.

Yan, Q., Yang, X., Cantone, A., Giebisch, G., Hebert, S. and Wang, T. (2008). Female ROMK null mice manifest more severe Bartter II phenotype on renal function and higher PGE2 production. *Am. J. Physiol. Regul. Integr. Comp. Physiol.* **295**, R997-R1004.

Yu, J., Carroll, T. J. and McMahon, A. P. (2002). Sonic hedgehog regulates proliferation and differentiation of mesenchymal cells in the mouse metanephric kidney. *Development* **129**, 5301-5312.

Yu, J., Valerius, M. T., Duah, M., Staser, K., Hansard, J. K., Guo, J. J., McMahon, J., Vaughan, J., Faria, D., Georgas, K. et al. (2012). Identification of molecular compartments and genetic circuitry in the developing mammalian kidney. *Development* **139**, 1863-1873.

SUPPLEMENTARY DATA

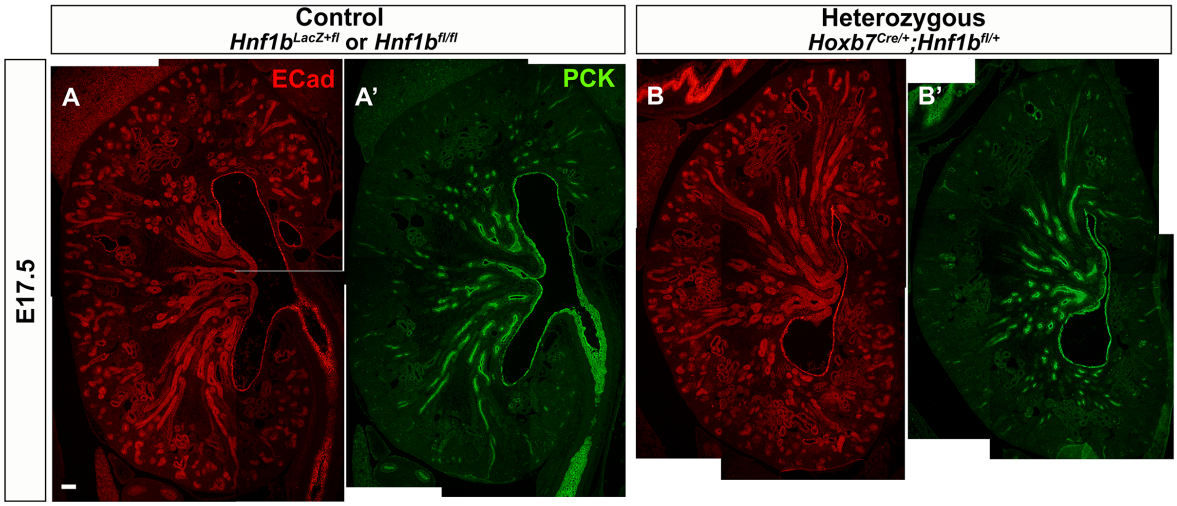

Supplementary figure S1: Comparative staining of collecting ducts and nephrons in control and heterozygous kidneys

Ecad and PCK staining of kidney tubules and collecting duct system, respectively show no difference between control (A, A') and heterozygous kidneys (B, B'). Scale bar, 100 μm.

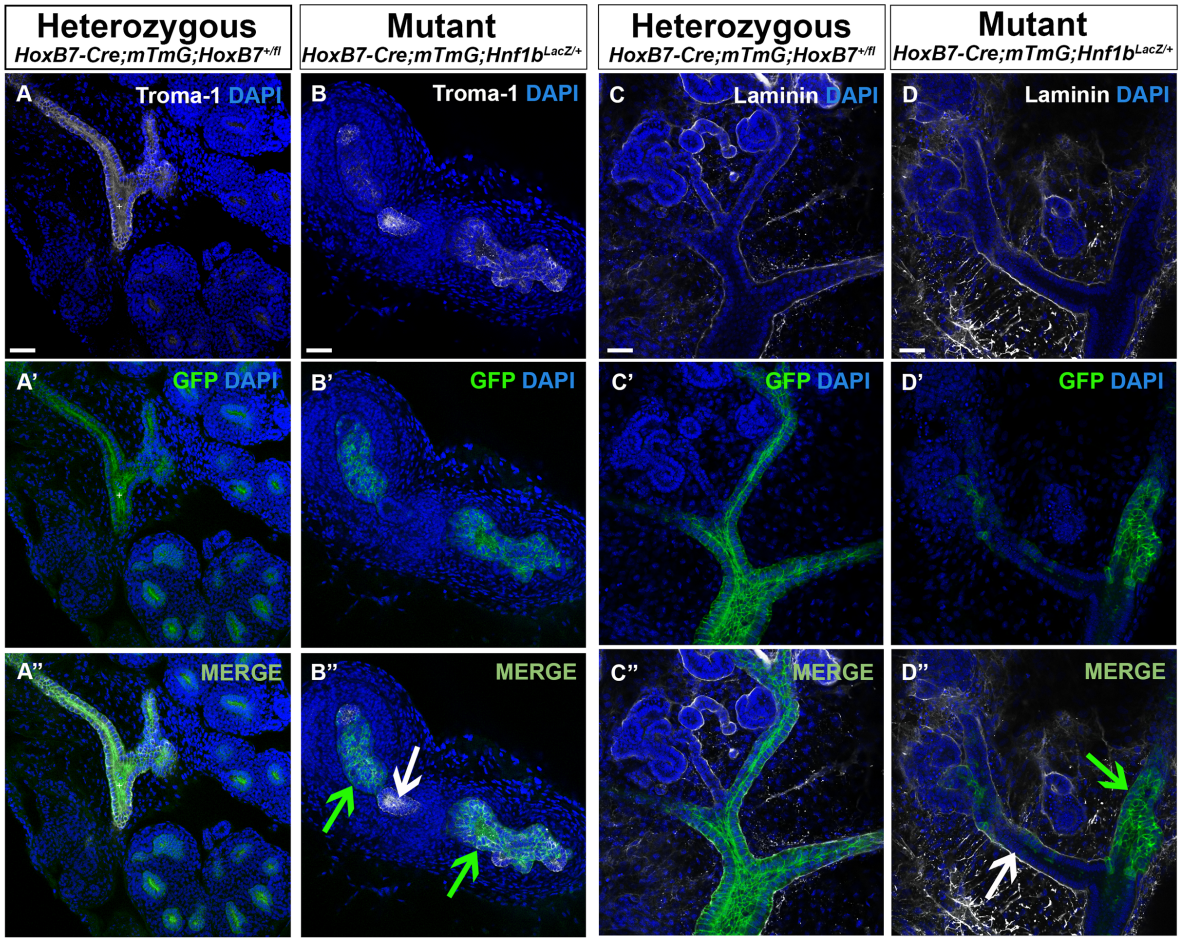

Supplementary figure S2: *Hnf1b* invalidation leads to loss of apico-basal polarity *in vitro*

Confocal images of Troma-1 (A–B'') and Laminin (C–D'') immunostainings after 5 days of culture show specific loss of the apical and basal markers in mutant ureteric bud regions (that are GFP-positive). White arrows, WT cells; green arrows, GFP+ cells. Scale bar, 50 µm

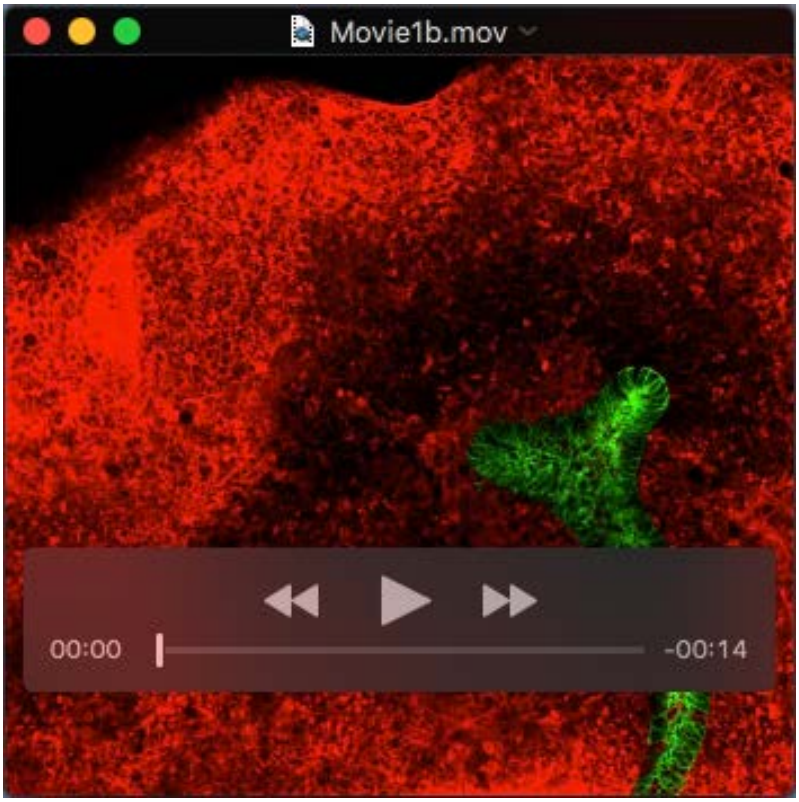

Supplementary Movie 1

Time-lapse imaging of *Hoxb7*$^{Cre/+}$*;mTmG;Hnf1b*$^{fl/+}$ kidney shows first branching events. Tip domain with active cell movements and trunk with lumen formation can both be seen. By the end of the movie, nascent nephrons (Red cells) are observed. One image is taken every 10 minutes. Green is mG expression in Cre expressing cells. Red is mT expression in Cre non-expressing cells. Mitotic cells can be easily detected as they become round before division.

Supplementary Movie 2

Time-lapse imaging of *Hoxb7*$^{Cre/+}$*;mTmG;Hnf1b*$^{fl/LacZ}$ kidney shows defective branching pattern. Tip domain show active cell movements but lumen in the trunk is barely visible. By the end of the movie, WT cells appear to be recruited at the UB tip domain and correctly formed nascent nephrons are observed. One image is taken every 10 minutes. Green is mG expression in Cre expressing cells. Red is mT expression in Cre-non expressing cells. Mitotic cells can be easily detected as they become round before division.

Supplementary Table 1:

A- Selected down-regulated genes in E15.5 mutant kidneys: Using the gene expression data available in Gudmap (www.gudmap.org), genes expressed in the UB, medullar and cortical collecting ducts but also in the urothelium were selected from the whole data set of 499 down-regulated genes with a FDR or adjusted p-value threshold of 0.05 and a fold-change cutoff value of 1 in a $\log_2$ scale. This reduced the whole list to 256 down-regulated genes.

Note that several genes express additionally in early nephron segment tubules.

B- HNF1B target genes down-regulated under the fold-change cutoff value of 1 in a $\log_2$ scale

C- Selected dowregulated genes containing HNF1B binding sites identified by ChIP-seq on E14.5 kidneys. Only are shown the genes containing strong HNF1B binding peaks identified by ChIP sequencing on embryonic kidneys (C.H. and S.C. unpublished data). The chromosomal location of binding peak score is indicated.

D- Complete list of up-regulated genes in E15.5 mutant kidneys

Click here to Download Table S1

Supplementary Table 2: Selected Gene ontology terms enriched in down-regulated and up-regulated genes in E15.5 mutant kidneys.

Click here to Download Table S2